EVALUATION OF THE DAMAGE TO THE BORAX CORPORATE HEADQUARTERS BUILDING AS A RESULT OF THE NORTHRIDGE EARTHQUAKE

Jerome F. Hajjar
DEPARTMENT OF CIVIL ENGINEERING
UNIVERSITY OF MINNESOTA
MINNEAPOLIS, MINNESOTA

David P. O'Sullivan
EQE INTERNATIONAL, INC.
SAN FRANCISCO, CALIFORNIA

Roberto T. Leon
SCHOOL OF CIVIL AND ENVIRONMENTAL ENGINEERING
GEORGIA INSTITUTE OF TECHNOLOGY
ATLANTA, GEORGIA

Brett C. Gourley
HAMMEL, GREEN AND ABRAHAMSON
MINNEAPOLIS, MINNESOTA

SUMMARY

The Borax corporate headquarters building was less than one year old when it sustained significant structural damage during the 1994 Northridge Earthquake. Seventy-five percent of its steel moment-resisting connections suffered severe brittle fractures. This report presents detailed documentation of the forensic investigation and repair design performed on this structure by EQE International immediately following the earthquake. It also presents the findings from a subsequent analytical investigation performed on the structure at the University of Minnesota. The two primary failure modes at the Borax building were column flange fracture, and pull-out of the girder flange from the column. The fractures are primarily attributed to a fundamental flaw in the standard code prescribed welded-flange bolted-web connection, and the extreme ground motion at the site. Other contributory factors are also identified. Additionally, the damage distribution suggests that greater energy input may be required to produce column flange fracture than girder flange pull-out. Results from a 3D nonlinear dynamic analysis using a site-specific accelerogram provide strong correlation with the observed damage, while elastic analyses, 2D analyses, and 3D static analyses show less correlation. While little evidence of yielding was found in the forensic study, the ductility demands obtained from the transient analyses indicate that substantial redistribution of forces may have occurred due to fracture or inelasticity, or a combination, and that this redistribution had a substantial effect on the final pattern of failures observed in the structure.

1. INTRODUCTION

The Borax corporate headquarters building, located in Valencia, California, suffered significant structural damage during the January 17, 1994 Northridge Earthquake. This four-story special moment resisting steel space frame structure, which was less than one year old at the time of the earthquake, required six months to repair at a total cost exceeding one-third of the original construction cost. This report summarizes the observed damage, damage evaluation, and repair design performed by EQE International immediately following the earthquake, and subsequent linear and nonlinear, static and transient dynamic analytical studies of this structure performed at the University of Minnesota. Towards the end of the report, correlations are made between the results from the computational study and the actual observed connection damage. Specifically, it is shown that results from a three-dimensional, second-order inelastic, transient dynamic analysis using an earthquake accelerogram generated for the Borax site provide strong correlation with the observed damage, while elastic analyses, two-dimensional analyses, and three-dimensional static analyses show significantly less correlation.

The macro-level frame analyses reported here form part of a larger research project at the University of Minnesota which included detailed micro-level continuum finite element analyses of typical damaged connections from the Borax building, as well as an experimental research program in which several full-scale specimens were tested cyclically. The test specimens, consisting of W27x94 steel girders framing into either side of a W14x211 column, were based on typical member sizes and connection details found in the Borax building. The University of Minnesota research focused primarily on the effect of the composite floor slab on the behavior of these steel moment frame connections. However, this document concentrates more specifically on a description of the observed connection damage to the building, the repair of the structure, and a correlation of this damage with the macro-level frame analyses. Sections 2 through 6 of this report outline the details of the site and geometry of the Borax building, the observed damage, and the retrofit methodologies. Sections 7 through 9 outline the details of the frame analyses and their correlation with the reported damage. Conclusions are drawn in Section 10.

2. BUILDING SITE AND PROBABLE GROUND MOTIONS

The Borax site, located at 26877 Tourney Road, is adjacent to Interstate 5 near the Valencia Boulevard exit. The site is approximately 23 km North of the epicenter of the earthquake (site coordinates: 34.4129 N; 118.5751 W), but 9.3 km from the closest point on the inferred rupture surface. Based on a review of the foundation investigation report prepared for the original design, the natural site soils consist of silty sand, sand, and silt which are firm and dense. The site was developed in 1985 by cut and fill to form a relatively level building site. The majority of the office building is located in a cut area, with only the northeast corner situated on fill. Fill material is less firm and consists of silty sand, sandy silt, clayey silt, and sand with some gravel and cobbles. The natural site soils are Pleistocene age fluvial terrace deposits extending to an

estimated depth of 150 feet. They are underlain by sedimentary rocks of the Plio-Pleistocene age Saugus Formation.

Shortly following the earthquake, Woodward Clyde Consultants were asked to develop a preliminary estimate of the ground motion at the Borax site during the Northridge Earthquake. Although it was recognized that this estimate would be based on limited available data, it was considered important to assist in the explanation of the unexpected extensive damage to the steel frames in the Borax office and laboratory buildings.

The Northridge Earthquake occurred on a southwest-dipping thrust fault beneath the San Fernando Valley. The rupture began at a depth of 19 km and propagated updip toward the northeast on a plane dipping 42° from the horizontal. The earthquake produced very large long period motions at the strong motion recording stations located within the northern margin of the San Fernando Valley and the adjacent Santa Susana Mountains. Additionally, recorded peak accelerations produced by the Northridge Earthquake were on average about one standard deviation above those predicted by the existing empirical attenuation relationships. The strong long period motions were attributed to the rupture directivity effect, caused in this case by the propagation of the rupture updip toward the north-northeast. The large long-period velocity pulse characteristic of the rupture directivity effect contains much of the energy released by the fault.

The nearest strong motion recording station to the Borax site is located at the Newhall L.A. County Fire Station site operated by the California Strong Motion Instrumentation Program (CSMIP). The Newhall site is located at the same distance (9.3 km) from the inferred rupture surface as the Borax site, but is approximately 4.9 km to the southeast. Another recording station, also operated by CSMIP, is located at Castaic Old Ridge Route, approximately 23 km from the inferred rupture surface, and 18 km to the north of the Borax site. The Newhall and Castaic time-history ground motions recorded by CSMIP (Darragh et al. 1994) are given in **Figures 2-1** and **2-2**. The recorded peak horizontal ground accelerations were 0.63g and 0.59g for the Newhall and Castaic sites, respectively. Similarly, the peak vertical ground accelerations were measured at 0.62g and 0.25g, respectively.

The recordings at the Newhall and Castaic sites formed the basis of the preliminary Borax site ground motion estimate. Response spectra generated from the Newhall and Castaic ground motion records are shown in **Figure 2-3**. The rupture directivity effect produced the large bump in the Newhall spectrum centered at a period of about 1.0 second. Also, the large peaks at periods of about 0.3, 0.7 and 1.0 seconds exceeded the median levels calculable from the existing empirical attenuation relations. Similar observations can be made from the response spectrum generated from the Castaic records. The preliminary estimate of ground motion at the Borax site was prepared in the form of a range of horizontal response spectra at 5 percent damping. This estimate is shown in **Figure 2-4** superimposed over the Uniform Building Code (UBC) response spectrum. While it was recognized that this estimated range was based on very preliminary technical information, this figure clearly demonstrates that for the period range near that of the

Borax building (approximately one to one and a half seconds), the site ground motions significantly exceeded those which form the basis of the building code.

Long after the Borax building had been repaired, SAC authorized the development of site specific ground motion time histories to facilitate analytical investigations of specific steel frame buildings damaged by the Northridge Earthquake. These time histories were generated by Woodward Clyde by combining two procedures; a low frequency procedure aimed at capturing rupture directivity effects, and a high frequency procedure intended to predict the large peaks associated with near-fault strong ground motions (Somerville, P. G. et al 1995). The generation technique was validated using the recorded ground motions from Northridge and other earthquakes. Subsequent to the development of these ground motions for the specified sites, Woodward Clyde generated one set of estimated time histories for the Borax site which was used in the analytical studies described later in this report. The resulting time histories are shown in **Figure 2-5**. There are two notable differences between these histories and those recorded at Newhall and Castaic. First, the peak accelerations in the north-south direction are significantly greater, while the peak east-west and vertical motions remain comparable. Second, and more importantly, the strong motions are concentrated into fewer, but longer period pulses.

3. BUILDING DESCRIPTION

The Borax Corporate headquarters building is a four-story steel frame office building designed in 1991 per the 1988 edition of the Uniform Building Code (UBC-88). It was built as part of a complex which includes an adjacent single-story steel frame research laboratory and a three-story reinforced concrete parking garage. The office building is basically rectangular in plan measuring approximately 187 by 110 feet and stands about 55 feet tall, excluding a small rooftop penthouse (**Figure 3-1**). The floor heights are typically 13'- 4", except for the ground floor which is 14'-6" tall. On each floor there is a 27 foot long by 24 foot wide projection at the center of the south wall. Also, the northeast corner of the floor diaphragms are notched to accommodate a stairwell. The only other significant irregularities occur in the second floor framing (**Figure 3-2**). At this level, there is a large opening in the diaphragm in front of the elevators, and a 24 foot curved projection along the west wall. Also, there is an irregularly shaped projection at the north end of the building which accommodates the entrance lobby. The framing over this lobby is located approximately 4 feet higher than the second floor.

The roof and floor framing for the building consists of 3-1/2 inch normal weight reinforced concrete over 2 inch deep metal decks. The metal decks are supported by steel wide-flange beams spaced at 10 feet. The beams span 30 or 40 feet between steel wide-flange girders or columns. The girders typically span 20 feet. The columns are typically supported by square reinforced concrete footings. Columns near the northeast corner of the building are supported on caissons to accommodate softer soil conditions. The ground floor is a 5 inch thick reinforced concrete slab-on-grade.

Lateral loads are resisted by special moment resisting frames located adjacent to each of the exterior walls. The frames are 4 bays wide in the north-south direction and 3 bays wide in the east-west direction. Fixity is provided at the base of the columns through embeddment in three foot deep grade beams which tie the column footings together. The girder material is ASTM A36 and the column material is ASTM A572 grade 50.

It should be noted that there is little redundancy provided in the Borax building's lateral load resisting system. As seen in **Figure 3-2**, only five of the ten columns along each north-south wall are included in the moment resisting frames. Also, although all four columns at each east-west wall are included in the moment frames, none of the building's eight interior transverse frames were designed to participate in resisting lateral loads.

Girder and column sizes used in the moment resisting frames are shown in **Figure 3-3**. The girder and column sizes are slightly larger in the east-west direction where there are fewer bays. As evident from this figure, the girder sizes in a given direction do not vary within any floor level. The girder sizes range from a maximum of W36x135 at the 2nd floor framing level in the east-west direction to a minimum of W24x55 at the roof in the north-south direction. In each moment frame, larger column sizes are used at the interior columns than at the ends. At each column location, two member sizes are used over the height of the building. The column segments are spliced using partial penetration groove welds located four feet above the second floor. The column sizes used in the moment frames in the Borax building are rather light compared to the girders and rely on the difference in column and girder minimum yield strengths to meet the strong-column weak-beam provisions of the code. In the north-south direction, the interior ground floor columns are W14x159 and the exterior columns are W14x132. Above the second floor, these sizes reduce to W14x145 and W14x120, respectively.

The pre-earthquake moment frame connections utilized flange stiffener (or continuity) plates with thicknesses specified as half of the girder flange thickness or 1/2 inch, whichever was greater. The design also specified extensive use of doubler plates in the column panel zones. The doubler plates were required at all but the roof level connections. The required thicknesses at interior column locations ranged from 7/8 to 1-1/4 inch. These thicknesses were achieved using doubler plates on both sides of the column web. The required doubler plate thicknesses at the end columns were only 1/4 or 3/8 inch, so only one side of the column web was thickened.

The exterior of the building consists of 4-1/2 inch thick architectural precast concrete spandrel and pier panels and glazing. As an architectural feature, glazing is substituted for the panels at the south building projection and at the northeast corner stairwell (see **Figure 3-1**).

4. EARTHQUAKE DAMAGE AND PRE-EARTHQUAKE MOMENT CONNECTION CRACKING

The initial post-earthquake damage survey of the Borax office buildings did not suggest that structural damage had occurred. The observed damage was limited to some cracking of interior full-height gypboard walls, a few fallen ceiling tiles, limited window breakage, and extensive toppling of office furnishings (**Figure 4-1**). In contrast, the adjacent lab building suffered obvious severe structural damage including failure and near collapse of a portion of the roof-diaphragm, noticeable permanent story drift, and broken precast panel connections. Consequently, the immediate concern was the stabilization and repair of the lab building.

After some of the office building's damaged ceiling and gypboard had been removed, and the office furnishings were uprighted, some of the fire-proofed structural framing was visible. By this time, column fractures had been found at several of the moment connections in the lab building, so there was heightened concern over the condition of the office building connections. At one second floor framing moment connection, a small separation in the fire-proofing was noted between the bottom girder flange and the column flange. The fireproofing was immediately removed revealing a pull-out failure of the bottom flange weld. Spot checking of adjacent columns, and at locations on other floors, confirmed that the problem was widespread, even though the fireproofing normally appeared undisturbed. Subsequently, removal of fire-proofing was ordered for all moment connections in the building. Within a week of the earthquake, extensive damage had been discovered of a nature never previously reported.

For the purposes of describing the damage to the moment connections, the identification system given in SAC Interim Guidelines (1995) will be used. The applicable SAC identifiers, as well as additional identifiers necessary to adequately describe the damage are shown below in **Table 4-1**.

Damage was found at 100% of the second floor, 93% of the third floor, 57% of the fourth floor, and 50% of the roof framing moment connections. This damage always occurred at the location of the girder bottom flange. No failures of top flange connections were noted. Cracking was noted in most of the top flange welds, however, as discussed later, it is believed that these cracks were formed during welding and were not earthquake related.

Two principal types of moment connection damage were found; girder flange pull-out, and column flange fracture. All of the observed fractures were brittle in nature, and the consensus opinion of the many researchers who viewed the damage was that the failures had occurred during one or two strong pulses.

The most common failure mode was girder flange pull-out. This was a complete or partial pull-out of the girder flange from the column flange and occurred in 56 locations in the building, approximately evenly distributed between the north-south and east-west frames. In 11 of these cases, the fracture initiated at the root of the girder flange weld, followed the heat affected zone

(HAZ) through the column flange base metal, and resurfaced on the column flange at the top of the bottom girder flange (Type C2*, **Figure 4-2**).

TABLE 4-1: MOMENT CONNECTION DAMAGE IDENTIFIERS

Damage Type	*Description*
C2	Column flange tear-out or divot
C2*	Column flange tear-out or divot where fracture returns to the column flange face at the top of the girder flange
C4	Full or partial column flange crack in the heat-affected-zone (HAZ)
C4*	Partial U-shaped column flange crack in the HAZ
C5	Lamellar tearing of column flange
G1	Buckled girder flange
G6	Yielding or buckling of girder web
W2	Crack through thickness of girder flange weld
P5	Partial depth fracture in doubler plate
P6	Partial depth fracture in web
P9	Severed column
S1	Partial crack at shear connection weld to column
S2	Fracture of supplemental weld between shear connection plate and girder web
S3	Fracture through shear connection plate at bolts
S7	Fracture through shear connection plate at start of supplemental weld

The remainder of the girder flange pull-out failures initiated at the root of the girder flange weld and followed a curved surface through the column flange base metal at the rear of the HAZ. The fracture surface normally extended well above the top of the girder flange, and in many cases returned to the face of the column flange (Type C2, **Figure 4-3**). Although the failure surfaces extended vertically through the column flange, they were generally curved, and those closely examined did not exhibit steps parallel to the column flange. For this reason, none of the fractures have been classified as Type C5 (lamellar flange tearing). Usually, the amount of material pulled from the column flange was greater near the middle of each leg of the girder flange, where the weld quality was highest. Where the fracture surface did not return to the column face, the failure was difficult to detect by visual methods. Usually, the only clue was a small gap between the flange weld back-up bar and the column face. Probing this gap with a thin gauge steel wire normally confirmed that there was a fracture, and that the depth of the fracture was two inches or more.

Column flange fractures occurred in 30 locations in the building, 29 of which were in the north-south frames. These fractures extended through the flange thickness, normally between the root of the girder flange weld and the top of the top continuity plate fillet weld. At 19 locations, the fractures extended across the full width of the column flange (Type C4, **Figure 4-4**). At the

remaining 11 locations, a U-shaped punching type failure occurred in which a horizontal fracture surface extended across the width of the girder flange then turned upward (Type C4*, **Figure 4-5**). In 23 cases (17 Type C4 and 6 Type C4*), the column flange fractures extended into the column web and doubler plates (Type P5 & P6, **Figure 4-6**). It should be noted that the cracks often did not propagate into the column web when first inspected, but by the time the connection was repaired, aftershocks had extended the cracks into the web. Also, when panel zone cracking was found extending from both column flanges, the columns were usually nearly severed. In at least one of these cases, the column was severed, however, the location was not documented. For this reason, none of the panel zone damage is classified as Type P9.

Samples of three Type C4 column flange fractures were removed then examined by a consulting metallurgist. The metallurgist concluded that one of the fractures initiated at the root of the girder flange weld. Another fracture apparently initiated at the toe of the top fillet weld between the continuity plate and column flange. The origin of fracture for the third sample was not clear. Mechanical testing and chemical analysis showed that the material met the ASTM A572 specifications. Micro hardness testing, however, showed increased hardness in the column flange in the vicinity of both the girder flange and continuity plate welds.

Fractures through the weld metal in the girder flange connection were observed at five locations (Type W2, **Figure 4-7**). In each case, the fracture of the weld metal occurred at the edge of the girder flange. The fractured weld metal always extended only partially across the flange width before running into the column flange and becoming a pull-out type failure (Type C2 or C2*). All five weld metal fractures were found in the east-west moment frames.

Although the observed moment connection damage was almost entirely brittle fracturing, some yielding was observed. Specifically, local buckling of girder flanges, flexural yielding of columns, and one case of girder web bending were noted. Local buckling of girder flanges (Damage Type G1) accompanied girder flange pullout or column flange fractures in seven locations (**Figure 4-8**). Most occurred with pullout type fractures in the east-west frames at the second floor framing level. The observed residual bending of columns occurred at the ground floor on line 10, however, the deformations were barely perceptible.

Failure of the girder flange connection or column flange fracture was often accompanied by damage to the shear connection plate. This damage took two forms. The most common was a short vertical crack of the shear connection plate, usually not more than 1/2 inch long, initiating at the start of the supplemental fillet weld to the girder web (Type S7, **Figure 4-9**). This type of damage was found at 23 locations. The second type of damage was a vertical crack of the shear connection plate through the bolt line (Damage Type S3, **Figure 4-10**). This occurred at 16 locations. It should be noted that in some cases when Type S3 cracks were first identified, they involved few bolt holes. However, by the time they were repaired, aftershocks had caused them to become significantly longer. Some of the Type S3 fractures extended more than two-thirds of the height of the plate. Since the cracking of the shear plates (either Type S3 or S7) left the

connection vulnerable to complete loss of vertical load carrying capacity, temporary pipe columns were installed as quickly as possible beneath each affected girder end.

Another common form of shear connection damage was cracking of fillet welds. Cracks were observed at the welds between the shear connection plate and column (Type S1), and at the supplemental welds between the shear connection plate and girder web (Type S2). The forensic inspection effort did not distinguish between these welds so, unless the specific damage is identifiable in the project damage photographs, this report uses "S1 or S2" to designate fillet weld damage. Cracking was more common at the supplemental girder web welds, and crack lengths were normally less than two inches.

The connection failure types found at each moment connection in the Borax building are shown in **Figures 4-11** and **4-12**. The damage is summarized by connection type, floor, and direction in **Table 4-2**. This table shows the total number of occurrences of each damage type, but cannot be used directly to determine the number of damaged connections because more than one damage type often occured at a connection.

TABLE 4-2: SUMMARY OF DAMAGE DISTRIBUTION

North-South Direction:

Floor	*C2*	*C2**	*C4*	*C4**	*P5&P6*	*W2*	*S1/S2*	*S3*	*S7*	*G1*
2nd	5	3	4	4	6	0	1	4	7	0
3rd	3	0	10	3	11	0	2	2	5	1
4th	4	3	4	4	6	0	0	0	1	1
Roof	10	0	0	0	0	0	0	0	0	0
Total	22	6	18	11	23	0	3	6	13	2

East-West Direction:

Floor	*C2*	*C2**	*C4*	*C4**	*P5&P6*	*W2*	*S1 or S2*	*S3*	*S7*	*G1*
2nd	12	0	0	0	0	2	2	7	5	5
3rd	4	5	1	0	0	3	6	3	4	0
4th	3	0	0	0	0	0	0	0	0	0
Roof	4	0	0	0	0	0	0	0	1	0
Total	23	5	1	0	0	5	8	10	10	5

Both Directions:

Floor	C2	C2*	C4	C4*	P5&P6	W2	S1 or S2	S3	S7	G1
2nd	17	3	4	4	6	2	3	11	12	5
3rd	7	5	11	3	11	3	8	5	9	1
4th	7	3	4	4	6	0	0	0	1	1
Roof	14	0	0	0	0	0	0	0	1	0
Total	45	11	19	11	23	5	11	16	23	7

The percentage of damaged connections at each floor in each direction were determined from **Figures 4-11** and **4-12** and the results are summarized in **Table 4-3**. In total, 75% of all of the bottom flange moment connections in the building failed. Upon review of the damage summary a few general observations can be made. First, the percentage of failure decreased with elevation. Next, it is evident that damage was more extensive in the north-south direction (86% of the connections were damaged versus 60% in the east-west direction). This is consistent with the stronger ground motion in that direction. Finally, 95% of all column fractures occurred in the north-south direction. Since the geometry in both directions is similar, this suggests that more energy input may be required to produce column fracture than the other connection failure types.

TABLE 4-3: PERCENT OF MOMENT CONNECTIONS DAMAGED AT BOTTOM GIRDER FLANGE CONNECTION

Floor	*North-South Direction*	*East- West Direction*	*Total*
2nd	100	75	100
3rd	100	63	93
4th	81	19	57
Roof	63	25	50
Total	86	60	75

Cracking of girder top flange welds was discovered by magnetic particle testing at over 80% of the building's moment frame connections. These cracks were not easily identified because the welds were heavily hammered, apparently by the welder's deslagging tool during construction. When first tested, only poorly defined shaded indications were visible. The weld surfaces in these areas were subsequently ground to remove surface distortions, and cracks up to 2 inches long were found (**Figure 4-13**). These cracks were not identified as earthquake damage because, in the opinion of the testing personnel, they were most likely shrinkage cracks formed during the original construction. In addition, the cracks were evenly distributed between the north-south and east-west frames and over the height of the building. If they were earthquake related, they should have been more prevalent in the north-south direction and at the lower floors.

Ultrasonic testing of the girder top flange connections also detected rejectable indications near the ends of the welds. These indications were widespread, occurring at about 70% of the connections, but were not identified as earthquake damage. They were believed to be result of slag inclusions caused by the use of weld dams during construction. Similar slag inclusions were positively identified at the ends of the girder bottom flanges (see Section 5). As with the shrinkage cracks, the even distribution of the UT indications throughout the building is further evidence that they were not earthquake related.

The girder top flange UT indications often occurred at flanges where shrinkage cracking was not found. Consequently, the total number of top flange welds with rejectable defects was over 95%.

Due to the extensive damage found at the girder to column connections, concern was raised as to the condition of the moment frame column splices. As a result, each of these column splices was exposed and inspected, but no damage was found.

In view of the extent of the damage to the moment connections, the exterior corners of the building were surveyed to determine if the building was out-of-plumb. The results were inconsistent due to the construction tolerances for the precast panels, but generally indicated that there was permanent drift at the roof in the order of 2 inches to the south, and a lesser amount to the west. Consequently, fireproofing was removed from one corner of two interior "leaner" columns to allow a more accurate measurement of interstory drifts. The interstory drift measurements are summarized in **Table 4-4.** These results clearly show permanent first story drifts of 1-3/8 inches to the south and 3/4 inch to the east. Lesser drifts were measured for the stories above. It should be noted that although these permanent deformations were significant, they were not visually perceptible.

TABLE 4-4: INTERSTORY DRIFT SURVEY OF INTERIOR COLUMNS (INCHES)

Column	*Direction*	*1st - 2nd*	*2nd - 3rd*	*3rd - 4th*	*4th - Roof*	*Total*
G-4	South	1.32	0.60	-	0.12	2.04
	West	0.72	0.12	-	-	0.84
J-7	South	1.32	0.60	0.12	0.12	2.04
	West	1.20	0.72	-	-	1.92

Due to the concentration of story drift at the ground floor, there was concern that the interior "leaner" columns may have residual bending deformations which would lessen their axial capacity. Hence, the leaner columns which had been exposed for the drift survey were also checked for straightness. This was accomplished by stretching a string from floor to floor and examining the space between the string and column. Checks were performed at the ground floor and second floor, but no distortion was detected.

The severity of damage to the moment connections along with the measured permanent building deformations raised concerns as to the condition of the non-moment beam and girder to column connections. Consequently, fireproofing was removed and these connections were inspected. Several were found to be damaged. The damage normally consisted of shear connection plates and beam or girder webs bent out-of-plane. In one case, a crack was found in a girder web emanating from the bottom bolt hole.

The final notable earthquake damage observation concerned the out-of-plane support for the precast panels. Several of the single-angle diagonal struts from the bottom of the panels to the floor above had buckled. This illustrates the limited ability of single-angles to resist compressive loads.

5. DAMAGE EVALUATION AND REPAIR RECOMMENDATIONS

Due to the extent of damage, the worsening condition due to aftershocks, and the magnitude of required repairs, the building was considered unsafe to occupy. Although Borax's emergency plans worked well, and deliveries were not interrupted, the temporary relocation of personnel was costly. Consequently, it was considered crucial to repair the facility as quickly as possible. Unfortunately, since the performance of the structure fell well outside the expectations of the building code, simply repairing the damage was not considered advisable. Before repair procedures could be recommended, it was necessary to evaluate the unexpected damage and determine potential causes. Several possible contributing factors were quickly identified. These included flaws in the original welding, possible embrittlement of the column flange HAZ, the configuration and welding of the continuity plates, the high demands on the connections, and most importantly, an apparent fundamental flaw in the code prescribed connection details for special moment resisting space frames.

Three principal flaws were consistently found in the original girder flange welding. These were inadequate fusion along the root of the welds, inadequate fusion at the ends of the welds, and inadequate fusion of the girder's bottom flange weld near the web. The lack of fusion is evident from the pictures in **Figure 5-1**. These are photos of portions of girder flanges removed from connections with Type C2 damage. In each case, the divot pulled from the column flange is still attached. The pictures show typical fracture surfaces where the divots were pulled from the column base metal. In each case, the entire face of the weld back-up bar is visible over a significant portion of the girder flange width. Where this occurs, there was obviously no fusion between the weld metal, back-up bar and column flange at the root of the weld. These flaws were clearly present in the original welds but were not discovered by ultrasonic testing (UT) during construction. This is not unexpected because, with the back-up bar left in place, it is extremely difficult to determine by UT whether there is complete fusion at the root of a weld.

Another significant problem evident from **Figure 5-1** is the orientation of the tabs at the edges of the girder flanges. These tabs were used to dam the weld metal at the edge of the flange to prevent spillage. They should have been oriented such that they formed a continuation of the joint preparation thereby allowing the weld to terminate beyond the joint as required by AWS D1.1. The resulting lack of fusion due to the trapped slag at the ends of the welds is evident.

The final observation from **Figure 5-1** is the lack of fusion near the beam web, which is also due to poor penetration and trapped slag. The presence of the beam web prohibits welding the bottom flange without stopping. Weld starts and stops often result in trapped slag and lack of fusion. It appears that the technique used in the original welding magnified the problem. The weld passes evidently started at the outside of the flange and progressed toward the web. This caused the welder to rotate his electrode near the web and push weld metal ahead of the electrode. The advancing pool of molten metal did not sufficiently heat the base metal and contributed to the observed lack of fusion.

Microhardness testing of samples of fractured column flanges showed higher values near the welds. Equivalent Rockwell C hardnesses of the HAZ's at the girder flange and continuity plate welds were as high as 26 and 24, respectively. This compares with an equivalent Rockwell C hardness of 16 away from the welds. This implies that the material was somewhat more brittle in these regions.

The continuity plates were half as thick as the corresponding beam flanges, or 1/2 inch thick, whichever was greater. As a result, assuming most of the girder force was transferred across the column flange into the continuity plate, the stresses in the continuity plate were greater than those in the girder flange. In addition, at the bottom girder flange connection, the elevation of the bottom of the girder flange matched that of the bottom of the continuity plate. Similarly, at the top girder flange connection, the elevation of the top of the girder flange matched that of the continuity plate. This offset between continuity plate and girder flange resulted in a complex state of stress in the column flange. It was felt that the local stress concentrations resulting from the continuity plates being thinner and offset from the girder flange may have been partially responsible for the observed column flange fractures.

The original design of the continuity plates called for complete joint penetration welds to the column flanges, however, fillet welds were substituted during construction. This created indirect load paths between the girder flanges and continuity plates which resulted in further stress concentrations. Since the column flange fractures were routinely found passing through the toe of the top fillet weld, it was felt that these stress concentrations may also have been a contributing factor in the column flange fractures.

Based on the range of probable ground motions at the site developed by Woodward Clyde (see **Figure 2-4**), it was obvious that the demands on the connections were significantly higher than those anticipated by the building code. It should be noted that other steel moment frame buildings located in the vicinity of the Borax corporate headquarters building also suffered significant structural damage. These included the three-story Santa Clarita City Hall building, and the two-story Automobile Club of Southern California building, which was eventually demolished. It was recognized that the extensive damage sustained by the few steel buildings in this area was largely due to the rupture directivity effect, however, this did not adequately explain the observed brittle failures. Regardless of the level of ground motion, any fracturing at connections was expected to be preceded by significant ductile deformation.

Recent testing at the University of Texas (Engelhardt, 1993) had produced pull-out type failures at low rotational demands which were very similar to dozens of the failures in the Borax building. The research concluded that the code-prescribed special moment frame connection may be inadequate. The damage observed at the Borax building, and at the dozens of other buildings damaged by the Northridge Earthquake, had apparently confirmed this finding. Consequently, repairing only to the building's pre-earthquake condition could not be recommended.

A computer model of the building was quickly developed and analyses were performed to determine the effect of the residual permanent story drifts on the future seismic performance of the building. After establishing that repairing the structure with these built-in deformations would not significantly reduce its capacity, repair recommendations were made. It should be noted that these recommendations were made just one month after the earthquake with the understanding that research by the structural engineering profession and the steel industry had begun and would likely last several months, or perhaps years. It was also recognized that this research would undoubtedly result in code changes governing the design of these connections and that these repair recommendations might or might not meet these future code provisions. Furthermore, it was acknowledged that additional measures might be required in the future.

The repair recommendations fell into three general categories; those intended to improve the quality of the connection welds, those intended to remove the known stress concentrations in the connections, and those aimed at reducing the stress in the girder flange welds.

Four measures were recommended to improve the quality of the flange connection welding. These were review of written welding procedures, strict inspection and nondestructive testing (NDT), peening of weld passes, and closely controlled pre-heat, interpass temperature, and cooling rate. The intent of the written welding procedure was to ensure that the fabricator, inspector, and most importantly the welder was aware of the acceptable welding parameters. Strict visual inspection was recommended to ensure that the approved welding procedures and all other AWS D1.1 requirements were followed. NDT was recommended for all completed welds, and at several stages during the weld repairs so that defects could be found and repaired when most accessible. Peening of weld passes was recommended as a means of stress relieving, which was considered necessary due to the highly restrained nature of the repair welds. Finally, careful monitoring of welding preheat, interpass temperature, and cooling rate was considered important to minimize the potential for embrittling the HAZ's.

It was apparent that high quality welds between the girder flanges and column were required (even for strengthened connections) if the desired inelastic rotations were to be achieved. Also, it was obvious that even the undamaged connections had significant flaws. Consequently, it was recommended that all undamaged bottom and top flange connections be rewelded.

In order to eliminate the known stress concentrations in the column flange at the girder flange weld, it was recommended that the existing continuity plates be replaced. The new plates would match the thicknesses of the girder flanges and would be welded to the column flanges with complete joint penetration welds. It was felt that this modification would reduce the risk of future column flange fracture.

Strengthening of the moment connections was recommended to reduce the likelihood of future flange pull-out type failures. In February 1994, however, available research on strengthened moment connections was limited. Significant increases in inelastic rotation had been achieved from flatwise cover plates, and ribs oriented vertically, although very few tests had been performed. Nevertheless, strengthening with vertical ribs was recommended. The vertical ribs

were chosen over the flatwise plates since they appeared to be more easily installed in this situation, would result in less massive welding to the column flange, and NDT appeared much more reliable.

6. REPAIR AND STRENGTHENING OF CONNECTIONS

The first step in the repair process was establishing the project welding procedures. This began within a week of the earthquake. Initially, it was thought that repair of column flange fractures could be accomplished by air-arcing through the column flange, beveling the top surface, and filling the gap with weld metal. Since this would involve building up a root opening about one inch thick with weld metal, it was decided to qualify the welding procedure by testing. The contractor performed the test weld using the shielded metal arc welding process (SMAW) with low hydrogen electrodes. The sample passed the procedure qualification tests, but the welding cost was high due to the low deposition rate. Consequently the contractor welded another sample using the flux-cored arc welding process (FCAW). Unfortunately, improper equipment was used and the sample failed the qualification testing. In the meantime, repairs were begun using the SMAW procedure. Proper equipment was brought to the site but the FCAW procedure still failed. The contractor then asked to use FCAW on "pre-qualified" joints with smaller root openings but, due to the lack of success with the larger root openings, was asked to run qualification tests. Several attempts were made to qualify a "pre-qualified" FCAW procedure by testing, but each time the welds failed to pass the required side-bend tests, even when the samples were aged before testing. Finally, a FCAW procedure using a notch-tough wire passed the qualification tests and was allowed to be used on the project.

It was disturbing that although "pre-qualified" procedures were used, and the welder was qualified for the process and position, several attempts failed to pass the qualification tests. Since the qualification test welds were performed by the contractors best welder, there was a low confidence level that the results could be routinely duplicated by the other project welders. Consequently, before welding in the building, each welder was asked to demonstrate his ability to produce an acceptable weld using the approved procedure. This test was performed on a 3/8 inch thick sample which was subsequently subjected to a bend test.

By the end of February 1994, repairs had begun and all of the strengthening recommendations had been approved by Borax. The minimum preheat and interpass temperature used for all repairs was 225°F, and the maximum interpass temperature was set at 600°F. Furthermore, post-weld cooling was limited to 100°F per hour. Electric heating elements were used to provide preheat, maintain heat during breaks, and to control cooling. They were chosen both to reduce fire risk, and to provide optimal temperature control.

The first step in the repair of the damaged bottom girder flange connections was the removal of a portion of the girder flange and web (**Figure 6-1**). This was required to provide access for column flange repairs. Where column flange damage did not extend through its thickness (Type

C2 and C2*), the damaged flange material was removed to sound metal. The exposed surface

was then thoroughly cleaned by grinding and examined by NDT. Next, the column flange was built back up with weld metal, ground flush, and examined by UT.

Where column flange fracture occurred (Types C4 and C4*), repairs were more complicated. First, a section of column flange, approximately 12 inches tall and slightly more than 1/2 of the width of the column was removed. A new section of plate was then inserted and welded to the top and bottom column flange surfaces and to the column web (**Figure 6-2**). Finally, the remaining portion of flange was replaced, and all welds were examined by UT. When the column fracture extended into the panel zone, a small hole was first drilled at the end of the crack to prevent propagation, and a one-inch radius was cut through the panel zone at the origin. The crack in the outside doubler plate was removed by air-arc gouging. The doubler plate was then cleaned-up by grinding, weld repaired using the column web as backing, and the surface of the weld was ground smooth (**Figure 6-3**). Next, the cracks in the inside doubler plate and column web were removed. Since the cracks in the these plates followed different paths, a large amount of material was sometimes removed from the inside doubler plate. The web and inside doubler plate were then weld repaired in a similar manner using the outside doubler plate as backing.

After the column repairs were completed, a new plate was fitted to replace the removed portion of the girder bottom flange. Complete joint penetration welds were then made in the flat position to the column and girder flanges (**Figure 6-4**). This required a vertical strut in the center of the new plate to prevent distortion. The back-up bars and weld extension tabs were removed, the flange surfaces were ground flush, and a reinforcing fillet weld was added at the root of the girder to column flange weld. Finally, new plate was fit-up and welded to replace the removed portion of beam web. Rat holes were employed to avoid welding over the new flange welds.

After the top girder flange welds were replaced, pairs of triangular rib plates were added at the top and bottom flanges (**Figure 6-5**). These plates were sized such that the plastic moment capacity of the ribs and girder flanges at the face of the column was 1.5 times the plastic moment capacity of the girder. The ribs were 6 inches tall, extended 12 inches along the girder, and varied in thickness between 1/2 and 1 inch. They were welded to the column flange with complete joint penetration welds and to the girder flange with double sided fillet welds.

It is important to note that nonstructural repair costs represented a significant percentage of the total. In addition to repair of cracked partition walls, replacement of broken glass, and adjustment of most of the door frames, architectural finishes had to be removed from the areas around each moment connection. Also, finishes damaged during the repair process required restoration. Affected items included metal stud and gypboard framed column covers, spray-applied fireproofing, suspended ceilings, carpeting, flooring, and painted finishes. In addition, some of the exterior precast panels had to be removed to provide access for welding. In these cases, the space between the column flange and exterior wall panel was just a few inches.

Other significant costs were related to safety precautions. Before cutting or welding in any area, it was necessary to cover all flammable materials to the extent possible. This was especially

necessary for air-arc gouging which can spew sparks and molten metal over a wide area. Since it

was not practical to create completely fireproof barriers, fire-watch personnel were stationed below each welder and were equipped with fire extinguishers. On several occasions, the fire-watch doused potentially dangerous fires. Another significant safety concern was smoke exhaust. In order to vent the smoke from the building, it was necessary to remove several windows on each floor. Fans and flexible ductwork were provided to remove smoke from each work point.

7. OVERVIEW OF THE FRAME ANALYSES

Several months after the forensic study and retrofit of the Borax building, nonlinear frame analyses of the structure were initiated at the University of Minnesota as part of a larger research program investigating probable causes of the damage to steel moment frame connections during the earthquake. The analyses consist of a series of studies predominantly examining the response of a selected moment frame in the structure. **Figure 7-1** illustrates a plan view of a typical floor. Moment connections are indicated by triangles at the girder ends. This macro-level analytical study focuses on the static and dynamic response of the west moment frame (Line 1) along the north-south axis of the structure (see **Figures 3-2** and **7-1**). This moment frame exhibited extensive connection failures on all floors upon inspection following the earthquake and is of interest since the dominant ground motion component at the building site from the Northridge earthquake was in the north-south direction, as discussed in Section 2.

7.1 TYPES OF ANALYSIS

Two models of the building are incorporated in this study: 1) a three-dimensional model of the entire structure, and 2) a simplified two-dimensional model of the west moment frame in the north-south direction of the structure. Linear elastic analyses, which are discussed in Section 9.1, are conducted to provide an indication of the forces used for design of the building, to locate areas of force concentration, and to compare the 2D and 3D results. The more general second-order inelastic analyses discussed in Section 9.2 provide more realistic values of force and displacement as well as a measurement of ductility. Within each of these categories, both static analyses (including equivalent lateral loads) and transient dynamic time history analyses were performed on the two structural models. **Table 7-1** summarizes the analyses conducted in this study.

FIGURE 7-1: FOUR-STORY BUILDING -- TYPICAL FLOOR PLAN

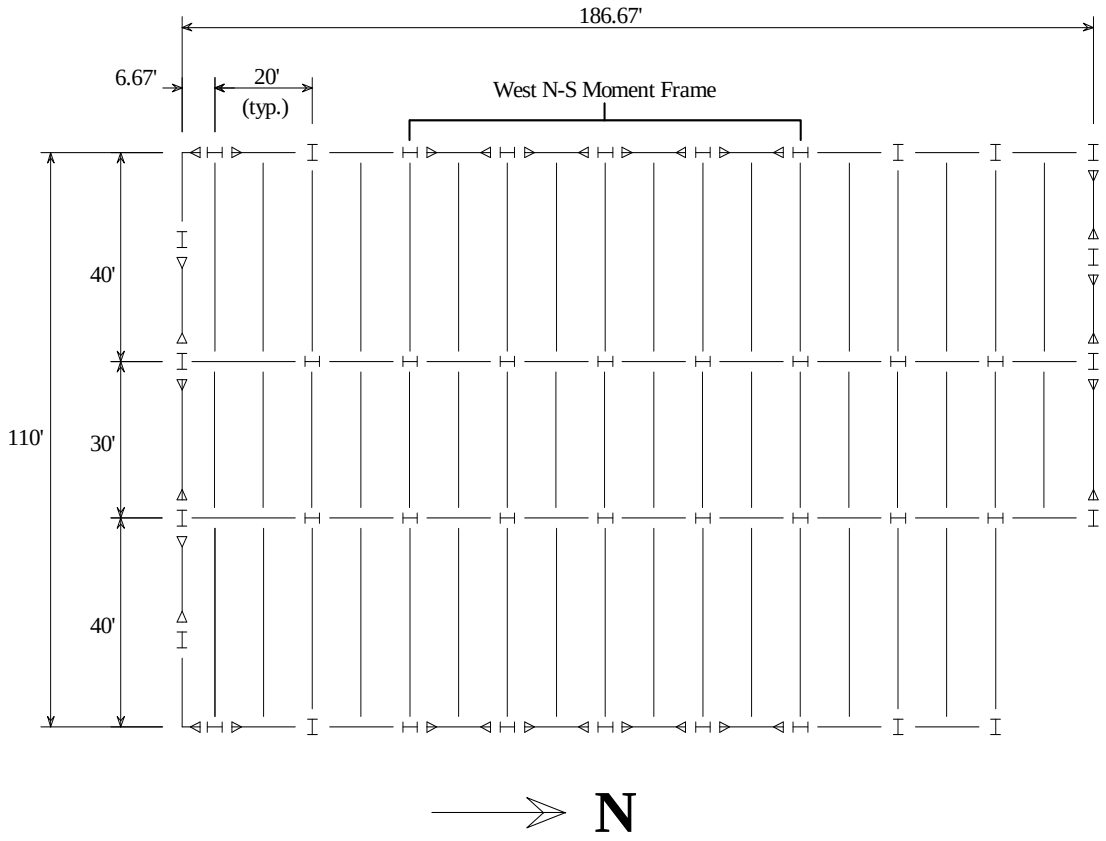

Dynamic loading was applied as base accelerations to the structure using two different accelerogram records. The first record consists of the site-specific accelerogram shown in **Figure 2-5**, provided for this project by Woodward Clyde Consultants (Woodward Clyde, 1994) (this accelerogram record is referred to as the "Site" record below). The portion of this record in which appreciable acceleration occurs spans approximately 15 seconds. Dynamic analyses were also performed using the accelerogram recorded at the Newhall Fire Station (**Figure 2-1**). The Newhall record exhibits appreciable accelerations for a duration of approximately 20 seconds. Note that in both the Site and Newhall records, the occurrence of significant vertical acceleration precedes the horizontal motion, and the north-south component of acceleration is clearly dominant in the Site record.

TABLE 7-1: SUMMARY OF MACRO ANALYSES

Linear Elastic Analyses:

1) Two-Dimensional Moment Frame
   - i) Equivalent Static
   - ii) Dynamic (Site record)
   - iii) Dynamic (Newhall record)
2) Three-Dimensional Structure
   - i) Equivalent Static
   - ii) Dynamic (Site record)
   - iii) Dynamic (Newhall record)

Second-Order Inelastic Analyses:

1) Two-Dimensional Moment Frame
   - i) Equivalent Static Pushover
   - ii) Dynamic (Site record)
   - iii) Dynamic (Newhall record)
2) Three-Dimensional Structure
   - i) Equivalent Static Pushover
   - ii) Dynamic (Site record)
   - iii) Dynamic (Newhall record)

7.2 FINITE ELEMENT FORMULATION

The analyses in this work were performed using a nonlinear analysis program developed at the University of Minnesota (Gourley and Hajjar, 1994). The frame is modeled using standard beam finite elements having twelve degrees-of-freedom per member. Each analysis incorporates a full Newton-Raphson iteration scheme to ensure equilibrium at each load or time step. Dynamic analysis is performed by implicit integration using the Newmark-Beta constant acceleration method with a typical time step of 0.01 seconds for the elastic analyses and 0.005 seconds for the inelastic analyses.

For the dynamic analyses, structural damping is assumed to be 5% of critical and proportional to the structure's mass and stiffness. The proportionality constants are obtained from the frequency values of the first two vibrational modes of the structure.

All members were input using centerline dimensions. However, in the west N-S moment resisting frame, rigid offsets are used to isolate the beam ends from the column centerlines. At each end of each girder in the moment frame, a rigid link was added, spanning between the girder end and the column centerline. The length of the link equals half the depth of the column into which the girder frames. The addition of these links had an almost imperceptible effect on

the stiffness of the structure (particularly for the 3D model). However, the rigid links permit the analysis forces and moments at the girder ends to be evaluated at the face of the column flanges rather than at the column centroid.

Geometric nonlinearity is incorporated in the nonlinear analyses through the use of a geometric stiffness matrix which accounts comprehensively for both the P-Δ and P-δ effects (Orbison, 1982; Gourley and Hajjar 1994). Using one finite element per steel member, this formulation yields accurate results for the range of column axial forces encountered in these studies (White and Hajjar 1991).

The plasticity model assumes that inelasticity is concentrated at the member ends. The bounding surface model is used for this study. This formulation incorporates two surfaces, an inner loading surface and an outer bounding surface, in three-dimensional force space ($P - M_y - M_z$) to model gradual yielding of the member end and to model the Bauschinger effect when a member undergoes cyclic loading (see (Hilmy, 1985; Zhao, 1993; and Gourley and Hajjar, 1994) for details of this force-space concentrated plasticity model). **Figure 7-2** illustrates the force-space bounding surface model at a member end experiencing inelastic behavior.

FIGURE 7-2: BOUNDING SURFACE MODEL IN TWO-DIMENSIONAL FORCE SPACE

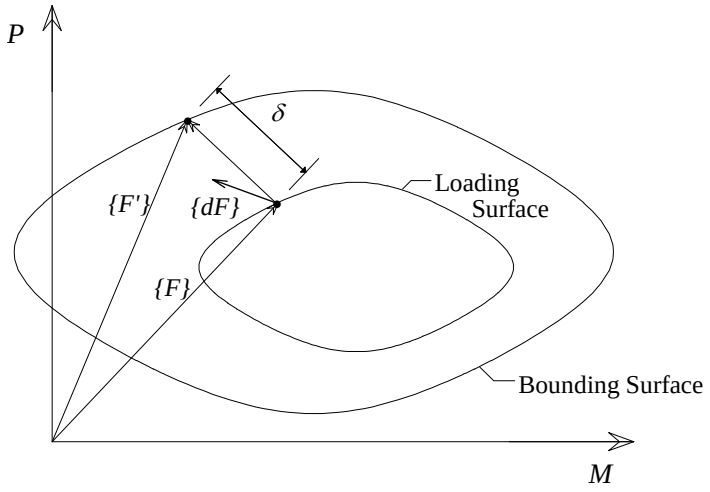

For the analyses in this report, the loading surface, which indicates the onset of inelastic behavior for a given member end, is set to a size of 0.5 times the size of the base cross-section strength surface. The equation used for this surface was developed by Orbison et al. (1982) to model the cross-section strength of wide-flange members. The smaller size of the loading surface relative to the full cross-section strength is used to account for early yielding due to effects such as residual stresses in the member. However, although inelastic behavior initiates when the force point at a member end contacts the loading surface, the member retains much of its stiffness until substantially more load is applied (as opposed to the abrupt loss of stiffness at yield that is typical in elastic-perfectly plastic models). As the forces at a member end increase, the force point (point $\{F\}$ in **Figure 7-2**) at a member end remains on the loading surface,

dragging it towards the bounding surface using a kinematic hardening formulation. This movement of the loading surface towards the corresponding bounding surface point $\{F'\}$ is shown in **Figure 7-2**. In this work, the bounding surface size has a value of 1.0 times the cross-section strength surface size. The member stiffness gradually decreases as the distance, δ, between the two surfaces decreases. When the force point and translated loading surface contact the bounding surface, the member end reaches a limiting stiffness, which is set to a small non-zero value to simulate the limiting value of stiffness exhibited in experimental force-deformation curves of wide-flange members (Hilmy, 1985). Once the bounding surface is contacted, it translates along with the loading surface. The kinematic hardening formulation is used primarily to model the Bauschinger effect exhibited in the force space behavior of steel wide-flange members (Hilmy, 1985).

In these analyses, neither the presence of the composite slab nor the behavior of the connections themselves is modeled explicitly. In addition, the effects of fracture are not accounted for. However, with respect to modeling the connection and panel zone stiffness and strength (neglecting fracture), this plasticity formulation has been calibrated by Hilmy (1985) and Zhao (1993) such that the gradual loss of stiffness modeled at a member end is representative of the behavior exhibited in experiments of complete steel beam-to-column connections (Popov and Stephen, 1972; Popov et al, 1985). Thus, the behavior of this fully-restrained connections is captured implicitly in this model.

8. THE STRUCTURAL FRAME MODELS

8.1 TWO-DIMENSIONAL MOMENT FRAME

Due to the preponderance of connection failures in the two north-south frames of the structure (see Section 4), the 2D analyses focus on the north-south moment frame on the west side of the structure. As discussed in Section 3, this frame consists of four stories and four bays, with all columns having a nominal yield strength of 50 ksi, and all girders having a nominal yield strength of 36 ksi. **Figure 8-1** illustrates an elevation of the frame showing the joint and element notation that will be referenced below. The circled joint indicates a connection that was damaged in the Northridge earthquake (see **Figure 4-11**). This connection exhibited a crack across the entire column flange thickness originating at the full penetration weld connecting the bottom flange of the girder to the column flange (see **Figures 4-5** and **4-6)**. This joint is examined in more detail in Section 9, as it serves as a representative connection in the frame.

FIGURE 8-1: NORTH-SOUTH MOMENT FRAME ELEVATION

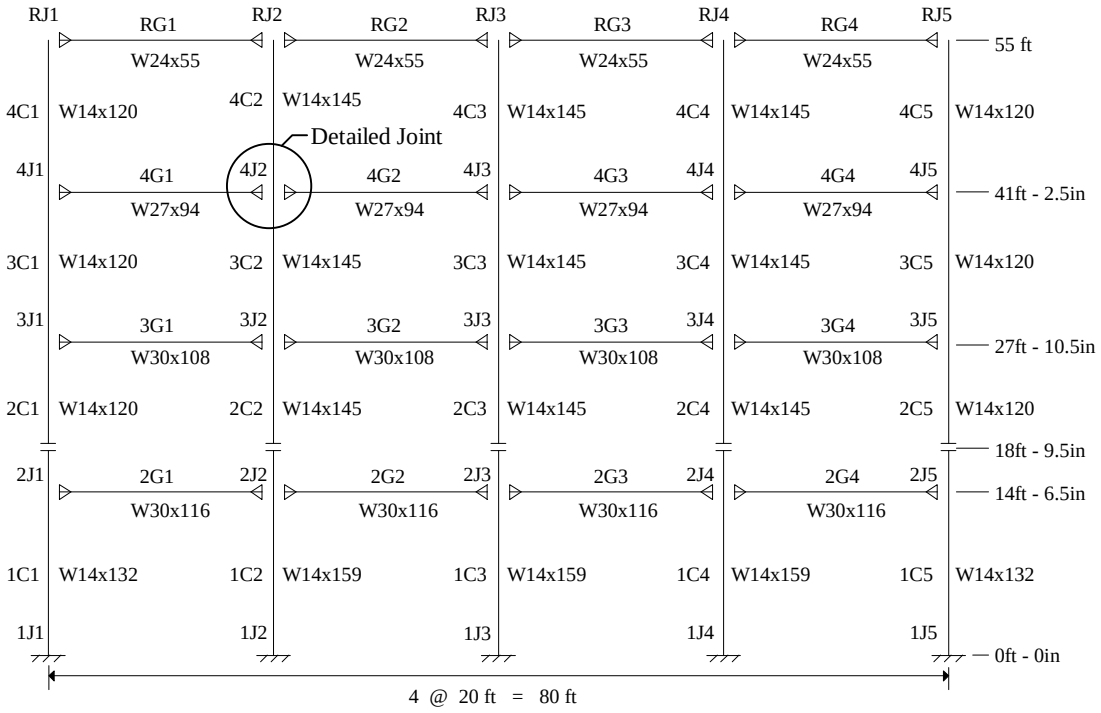

For these macro-analyses, bare steel properties were used for all members. To model the behavior of the complete structure realistically in the 2D frame, a stack of four columns was connected to the moment frame by pinned girders, and additional mass and dead load were applied to the joints of this column stack. The tributary mass and dead load of this frame at each floor in the 3D building (minus the amount on the frame itself) were added to the "leaner" columns of the add-on stack. This amounts to adding approximately 36 percent of the previously unassigned floor mass and floor dead load to the leaner column stack (the remaining mass is assumed to affect the other three moment frames of the structure). The effect of this extra column stack on the stiffness of the frame is minimal since the leaner column stack is pinned at the base and pin-connected to the frame. The moment frame shown in **Figure 8-1** was used for all 2D analyses. Note that the fully restrained connections in the southwest corner of the structure (see **Figure 7-1**), which are included to support the cantilevered floor, are not incorporated into this 2D model even though they are in the plane of the frame, as the column and girders are much smaller and the effect of these connections is expected to be negligible for lateral load resistance.

Eigenanalysis of the 2D moment frame shows that the first three vibrational mode shapes are typical: the fundamental mode is a sway mode, with a period of 1.23 seconds and maximum displacement at the roof; the second mode is a whiplash mode with a period of 0.446 seconds and a maximum displacement at level two; and the third mode has a period of 0.270 seconds and forms an "S" shape. The fundamental period compares reasonably well with that computed in the 3D model discussed in the next section.

The equivalent lateral loads used in the static analyses (see Section 8.3) were based on the period of vibration, *T*, computed using UBC-88 Method A. For steel moment frames, this period is calculated as:

$$T = 0.035 \cdot h_n^{3/4} \qquad (8\text{-}1)$$

where h_n is the height of the building in feet. For the structure in this report, which has a height of approximately 55 feet, Eq. (8-1) results in a period of 0.707 seconds. This period is about one half of the north-south direction fundamental period of vibration computed by an eigenanalysis of the 3D structure (see Section 8.2). The resulting equivalent lateral loads used for the static analyses in this report were not reduced by 20% as would be permitted by the UBC when the fundamental period computed by Method A is substantially less than that determined by eigenanalysis. It should be noted, however, that this reduction was apparently used for the design of the building (the more conservative load values were chosen for use in this study to contrast with the dynamic loading).

8.2 THREE-DIMENSIONAL STRUCTURE

The three-dimensional model seeks to simulate the actual structure with a minimum number of simplifications. All of the columns, girders, and beams of the main structure were included in the model (see **Figure 7-1**), although the single level lobbies on the north and west facades, the annex on the south facade, and the penthouse at the south end of the building were neglected. Additionally, stairwells, elevator shafts, and partitions were not modeled explicitly. All of the beams and the appropriate girders with simple shear connections were released at their ends to prevent major-axis moment transfer to framing girders and columns. The columns in each of the four moment frames were fixed at their bases while the remaining columns, those carrying only gravity load, were pinned at their bases.

To simulate the rigidity of the concrete floor slab and stairwells, additional stiffness was added to the structure by means of horizontal cross-bracing between the columns at each floor level. Using an eigenanalysis, the periods of the first and second modes of vibration of the stiffened 3D model are 1.44 and 1.37 seconds. These two modes are both essentially fundamental sway modes -- the first mode shape is the primary mode in the east-west direction and the second mode shape is the primary mode in the north-south direction of the structure. As mentioned

previously, the 1.37 second period of vibration in the north-south direction compares well with the 1.23 second period of the 2D model.

8.3 APPLIED LOADING

8.3.1 STATIC LOADING

As discussed in Section 5, analyses were performed during the forensic investigation to determine whether residual story drifts would significantly affect the capacity of the structure. The details of all load calculations used in that study were adhered to here as much as possible in the both the static and the transient dynamic analyses discussed below**.** Static analyses were performed on the 2D and 3D structures using an equivalent lateral load procedure and the following load combination:

$$1.2 \cdot D + 0.5 \cdot L + 1.5 \cdot E \tag{8-2}$$

where *D*, *L*, and *E* denote dead load, live load, and equivalent lateral earthquake load, respectively.

Factored dead and live loads are applied at the columns and at the mid-spans of the girders in the 2D frame. For the 3D building, factored dead and live floor loads are applied as distributed loads to the beams, and factored dead loads due to the curtain wall are applied as point loads to the perimeter columns. The loads are applied nonproportionally for the static nonlinear analyses, with the gravity load applied prior to the lateral load.

The equivalent lateral loads were calculated using the UBC-88 equivalent static lateral load procedure, as per the computations performed as part of the forensic investigation of this structure. The UBC-88 procedure entails computing a design base shear and distributing this shear vertically along the height of the structure. The base shear is given by the formula:

$$V = \frac{Z \cdot I \cdot C \cdot W}{R_w} \tag{8-3}$$

The parameter *Z* represents the seismic zone factor; *I* is an importance factor; *C* is a coefficient which is a function of the soil conditions and the period of the structure; *W* is the dead load of the structure; and R_w is a factor representing the ductility of the structural system. The site coefficient, *C*, is given by:

$$C = \frac{1.25 \cdot S}{T^{2/3}} \tag{8-4}$$

where *S* is a soil coefficient, and *T* is the fundamental period of the structure, calculated above in Eq. (8-1) as 0.707 seconds. For a soil coefficient, *S*, equal to 1.0, the site coefficient, *C* is 1.58. The value of *S* and the values for the remaining parameters in Eq. (8-3) are as follows:

$$Z = 0.4 \qquad I = 1.0 \qquad W = 8770 \text{ k} \qquad R_w = 12$$

Substituting these values into Eq. (8-3) results in a total design base shear of 465 k. Since there are two moment frames along the north-south axis of the building, the shear is divided by two and then distributed vertically on the moment frame as per UBC-88. The resulting loads at each level are shown in column 2 of **Table 8-1**. The frames are loaded at the joints indicated in column 3 (see **Figure 8-1**) by the amounts indicated in columns 4 and 5 for the 2D and 3D frames, respectively.

TABLE 8-1: EQUIVALENT LATERAL LOADS

Floor Level	*Total Equivalent Lateral Load (kips)*	*Loaded Joint (Figure 8-1 Notation)*	*2D Joint Load (kips)*	*3D Joint Load (kips)*
2	22.8	2J1	22.8	23.9
3	40.2	3J1	40.2	42.2
4	59.2	4J1	59.2	62.2
Roof (R)	110	RJ1	110	115

For the 2D frame analysis, the loads in column 4 of **Table 8-1** are multiplied by the load factor 1.5 and applied to the 2D frame at the joints indicated in column 3. For the 3D structure, the equivalent lateral loads are applied so as to induce an extra amount of torsion in the structure. To account for accidental torsion, UBC-88 requires that the center of mass of the structure be moved 5 percent of the plan dimension in the direction perpendicular to the loading. A simpler means of inducing accidental torsion into the structure was used by applying 5 percent larger lateral loads to one of the north-south moment frames. Therefore, 52.5 percent of the total factored lateral load at each floor level is applied to one of the north-south frames (column 5 of **Table 8-1**), and 47.5 percent to the other. Additionally, the effect of out-of-plane loading is included by applying 30 percent of the factored lateral loads to the frames in the east-west direction (17.5 percent to one east-west frame and 12.5 to the other). Lateral loads are applied directly to the four moment frames in the directions shown in **Figure 8-2**. The magnitudes of the loads are given as a coefficient times *L*, the total equivalent lateral load for a given floor in a given direction (e.g., column 2 of **Table 8-1**, multiplied by the load factor of 1.5).

8.3.2 DYNAMIC LOADING

For the dynamic analyses, gravity loads were applied to the 2D and 3D structures using the following load combination:

$$1.0 \cdot D + 0.5 \cdot L \qquad (8\text{-}5)$$

In addition to the gravity loads, base accelerations were applied to the structure using the Site and Newhall accelerogram records discussed in Sections 2 and 7. All three components (north-south, east-west, and vertical) of each accelerogram were applied to the 3D structure, while only the north-south and vertical components were applied to the 2D moment frame. The accelerograms act in directions parallel to the main axes of the structure. The gravity loads were applied quasi-statically over the first 0.5 seconds of the records, which contain little or no acceleration. This duration of time is sufficient to apply the full gravity loads gradually without inducing noticeable dynamic effects.

FIGURE 8-2: EQUIVALENT STATIC LOADING OF THE 3D STRUCTURE

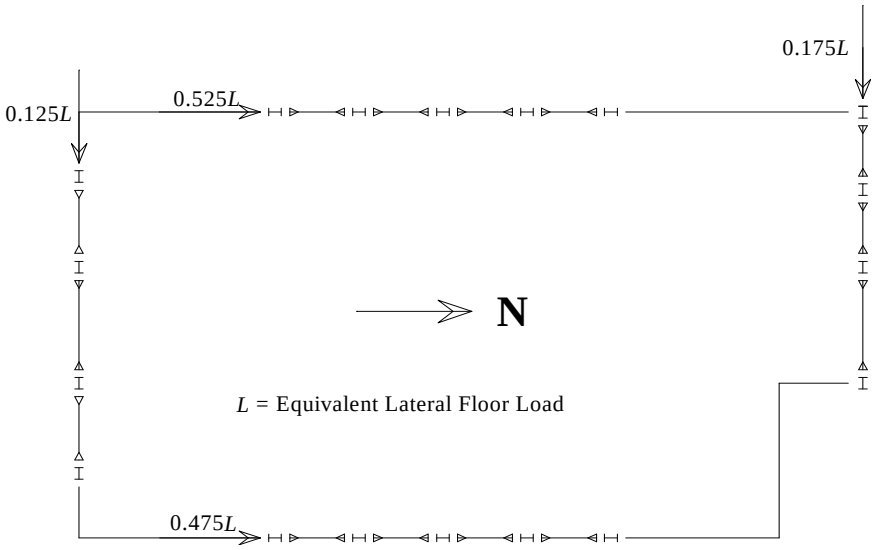

9. ANALYSIS RESULTS

9.1 LINEAR ELASTIC ANALYSES

The linear elastic analysis portion of this work examines the two- and three-dimensional response of the north-south moment frame of the structure to the three load cases discussed earlier: 1) equivalent static lateral loading; 2) dynamic loading using the Site record; and 3) dynamic loading using the Newhall record. The primary objectives of the elastic analyses are to: 1) examine the design of the moment frame to determine the amount of reserve capacity of the members (or lack thereof) when subjected to design equivalent static loads and the Northridge ground motions; 2) examine the magnitude of the axial forces in the columns; and 3) correlate failure patterns in the actual structure with the results of the elastic analyses.

For each of the six elastic analyses performed (see **Table 7-1**), three primary results are obtained. First, stress ratios are computed for all members of the frame. The stress ratios serve as an estimate of the amount of reserve capacity (if any) in the members, and they provide a means of correlating the analyses with actual failure locations in the structure in the event that connection fractures occurred prior to significant inelastic redistribution in the frame. Second, the axial forces in the columns are studied to determine whether the columns may have been put into tension during the earthquake. The third set of results focuses on the response of the beam-to-column joint isolated in **Figure 8-1**. This data provides a further comparison of the two models and will indicate the magnitude of elastic forces imparted by the two dynamic load cases.

9.1.1 LINEAR ELASTIC STRESS RATIOS

Elastic stress ratios are computed for each member end using the following formula:

$$Stress\ Ratio = \frac{P/A + M_y/S_y + M_z/S_z}{f_y} \tag{9-1}$$

The numerator of Eq. (9-1) represents the stresses due to axial force, weak axis bending moment, and strong axis bending moment (for the two-dimensional frame, the weak axis bending term is zero). The combined stress due to these actions is then normalized by the yield strength of the material to provide an estimate of the amount of residual elastic strength at a given member end. For the 2D analyses, a ratio of 1.0 for a wide-flange section provides a reasonable limit of this residual elastic strength. For the 3D analyses, a stress ratio of 1.0 in general does not necessarily indicate the onset of significant inelasticity in the member. However, for the wide-flange members in the moment frames of this structure, the out-of-plane effects are generally small, as the members framing in out-of-plane tend to be pinned.

Figure 9-1 illustrates the stress ratios for each of the member ends for the three analyses of the two-dimensional frame. Since rigid links are used at the ends of the girders, the girder stress ratios are essentially evaluated at the faces of the columns into which they frame. The top number for each end represents the stress ratio from the static analysis, and the bottom two numbers represent the stress ratios for the dynamic analysis using the Site and Newhall accelerogram records, respectively. The dynamic analysis values are member maximums over the entire record and do not necessarily occur concurrently in all of the members. Similar results for the north-south frame of the 3D model are shown in **Figure 9-2**. Note that the entire 3D structure has been analyzed in these cases, but only the members in the north-south moment frame of Line 1 are shown.

FIGURE 9-1: MAXIMUM LINEAR ELASTIC STRESS RATIOS --
N-S MOMENT FRAME OF 2D STRUCTURE

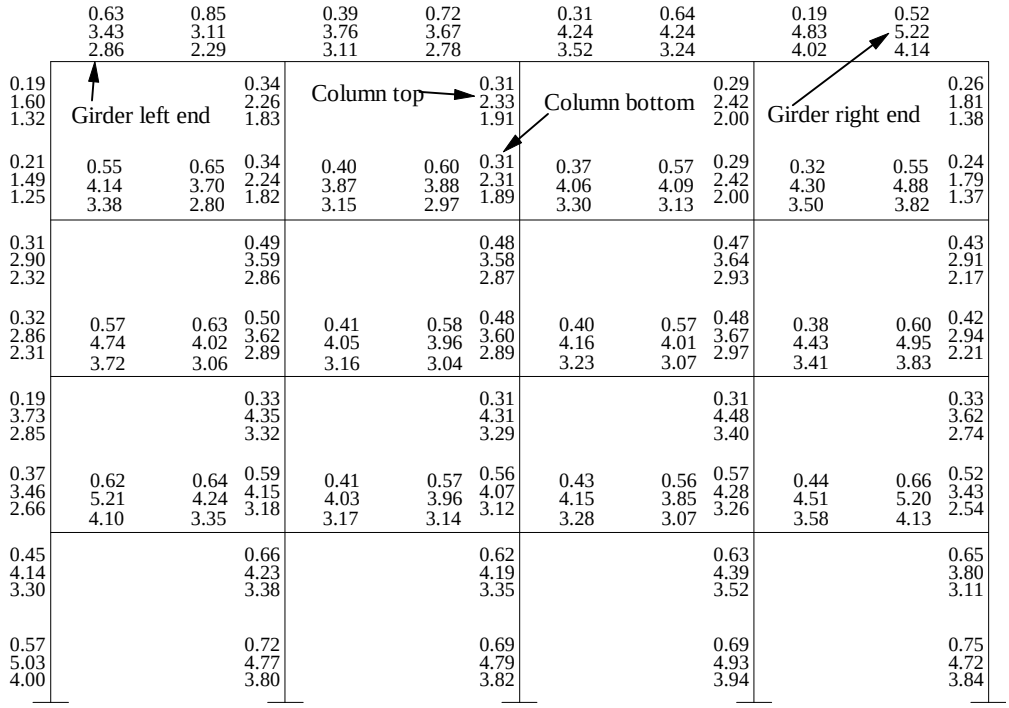

1) Equivalent Static

2) Dynamic -- Site Record

3) Dynamic -- Newhall Record

A number of general observations may be made from **Figures 9-1** and **9-2**. As expected, the equivalent static analysis generally produces stress ratios that are less than one in the members in both models, which verifies that the design complied with the applicable provisions of the seismic building code. In fact, this structure's design was controlled by drift, thus explaining the relatively low stress ratios resulting from the elastic static analyses (and recall from Section 8.1 that the original design apparently used equivalent lateral loads with magnitudes reduced by an additional 20% from the more conservative values chosen for use in the present study). As may be expected, the dynamic loading, for which the forces are, of course, not reduced by R_w, induces higher stresses than the equivalent static loading, especially for the stiffer 2D moment frame. Additionally, the Site accelerogram generally produces larger stress ratios than the Newhall accelerogram. The stress ratios shown in the dynamic analyses occurred over extensive time periods and did not merely occur at isolated points in time. The maximum stress ratio values for each analysis are shown in **Table 9-1**. For both models, the dynamic analyses produce stress ratios that are often 4 to 5 times the static values. These results indicate that the structure potentially had to dissipate a large amount of seismic energy during the Northridge earthquake in order to preclude extensive member failure.

FIGURE 9-2: MAXIMUM LINEAR ELASTIC STRESS RATIOS --
N-S MOMENT FRAME OF 3D STRUCTURE

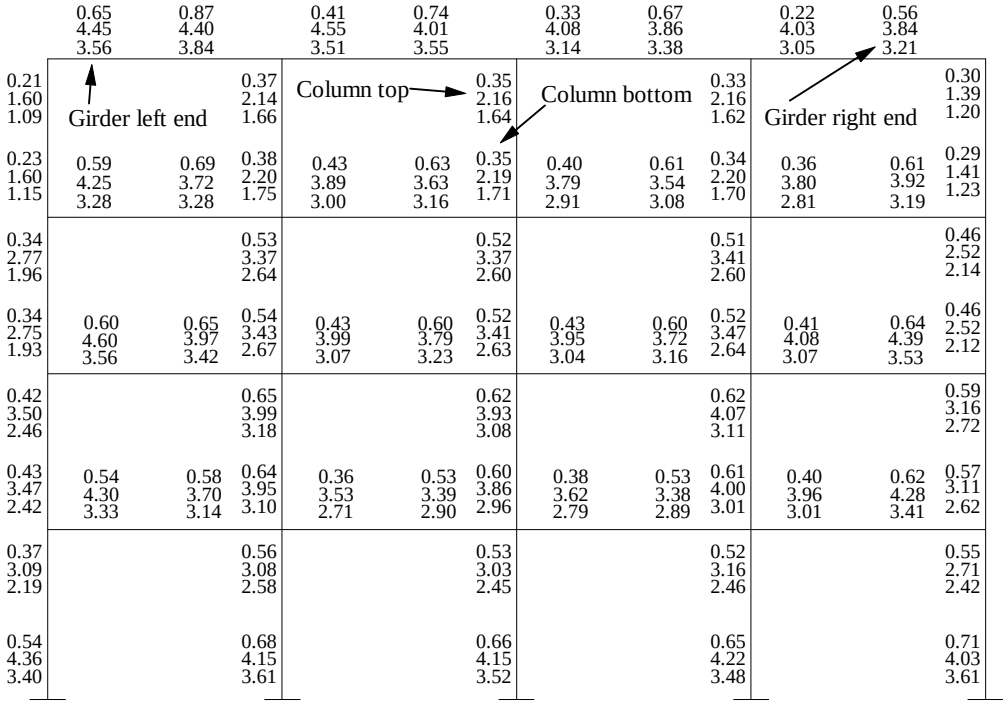

1) Equivalent Static
2) Dynamic -- Site Record
3) Dynamic -- Newhall Record

TABLE 9-1: MAXIMUM LINEAR ELASTIC STRESS RATIOS

Structure / Analysis	*Maximum Stress Ratios*	*Member (Figure 8-1 Notation)*
2D / Equivalent Static	Girders: 0.85 Columns: 0.75	RG1 1C5
2D / Dynamic (Site Record)	Girders: 5.21 Columns: 5.03	2G1 1C1
2D / Dynamic (Newhall Record)	Girders: 4.14 Columns: 4.00	RG4 1C1
3D / Equivalent Static	Girders: 0.87 Columns: 0.71	RG1 1C5
3D / Dynamic (Site Record)	Girders: 4.60 Columns: 4.36	3G1 1C1
3D / Dynamic (Newhall Record)	Girders: 3.84 Columns: 3.61	RG1 1C2

The static analyses often show the highest girder stress ratios near the top of the structure, corresponding to the large equivalent lateral load there (of course, the ends of the girders on the side of the load application, i.e., the south side, show larger stress ratios than girder ends away from the side of the load application). The 2D dynamic analyses show the girder stress ratios tapering off towards the top of the structure, and exhibiting a bias towards having higher stress ratios at the exterior column lines. The 3D dynamic analyses show the largest girder stress ratios to be scattered throughout the frame, with generally little bias between exterior and interior columns, or between girders on different floors. The largest column stress ratios generally occur at the base of the structure for all analyses and gradually taper off in higher floors.

9.1.2 TENSILE AXIAL COLUMN FORCE

Some investigators have suggested that tensile axial force may have contributed to the brittle connection failures in the Northridge earthquake. Both the 2D and 3D linear elastic analyses indicate that the exterior columns of the frame (column lines 1 and 5 in **Figure 8-1**) exhibit a net tensile force at some point in the dynamic load history for both the Newhall and the Site accelerogram records. Very few interior columns of the moment frames (column lines 2, 3, and 4 in **Figure 8-1**) ever experience a net tensile axial force.

It is instructive, however, to examine the effect of tensile axial forces induced specifically by dynamic loading. Although these tensile forces may not produce net tension in a column, the resulting axial compressive force in the column may be close to zero. To investigate this effect, the forces due to the static gravity loads ($1.0D + 0.5L$, see Eq. 8-5) are compared to the maximum values of the effective dynamic tensile axial forces (i.e., all additional axial forces due to dynamic loading) for each column in the moment frame. **Table 9-2** shows the results from each linear elastic dynamic analysis. The first column of values in the table for each analysis lists the maximum axial forces over the duration of the analysis (i.e., the force due to gravity loads plus the maximum dynamic tensile force). If the maximum dynamic tensile force exceeds the compressive force due to the static gravity load, this maximum force will be positive (i.e., tensile). The second value in the table expresses the maximum tensile dynamic force as a percentage of the force due to the gravity load. For example, column 1C1 is subjected to a static gravity force of -446 k. For the 2D Site analysis, the maximum net force in this column is 1137 k. The effective dynamic force causing this force is equal to 1583 k (i.e., 1137 k minus -446 k), which is 3.55 times or 355 percent of the force due to the static gravity load

Table 9-2 indicates that although few columns exhibit net tensile forces during the dynamic analyses, the minimum compressive force for the columns that are not subjected to net tensile forces is generally much smaller than the force due to the gravity loads alone. In all four analyses, the majority of the maximum dynamic tensile forces are over 80% of the compressive force due to gravity loads. Between the two dynamic records, the Site record produces larger tensile forces due primarily to the larger ground accelerations (compare **Figures 2-1** and **2-5**). Of course, the forces seen in the actual structure probably reflect the effects of inelastic

redistribution. However, in Section 9.2, it is shown that, while material inelasticity dissipates much of this excessive dynamic tensile force, the columns of this frame still exhibit small compressive, or even tensile, axial forces for large durations of time during the seismic excitation. In addition, this trend worsens if one were to compare the maximum axial forces from these analyses to the forces generated exclusively from the dead loads (i.e., a load combination of 1.0*D* rather than 1.0*D* + 0.5*L*), which would yield values of the gravity load which probably better represent those actually imposed on the structure at the time of the earthquake.

TABLE 9-2: LINEAR ELASTIC TENSILE AXIAL COLUMN FORCES
(NEGATIVE FORCE VALUE INDICATES COMPRESSION)

Column Notation (see Figure 8-1)	*Gravity Load, GL (k) 1.0D + 0.5L*	*2D Dynamic (Site)*		*2D Dynamic (Newhall)*		*3D Dynamic (Site)*		*3D Dynamic (Newhall)*	
		Max. force (k)	*% of GL*	*Max. force (k)*	*% of GL*	*Max. force (k)*	*% of GL*	*Max. force (k)*	*% of GL*
1C1	-446	1137	355%	644	244%	667	250%	620	239%
1C2	-474	-106	78%	-109	77%	-127	73%	-160	66%
1C3	-460	-117	75%	-172	63%	-141	69%	-192	58%
1C4	-472	20.2	104%	-87.3	82%	-80.9	83%	-131	72%
1C5	-452	1003	322%	862	291%	827	283%	476	205%
2C1	-331	721	318%	380	215%	466	241%	398	220%
2C2	-351	-87.6	75%	-113	68%	-109	69%	-131	63%
2C3	-341	-84.1	75%	-126	63%	-102	70%	-140	59%
2C4	-350	-11.6	97%	-94.5	73%	-69.6	80%	-116	67%
2C5	-335	599	279%	527	257%	522	256%	296	188%
3C1	-217	351	262%	165	176%	237	209%	179	182%
3C2	-228	-56.1	75%	-89.0	61%	-72.0	68%	-93.5	59%
3C3	-223	-51.8	77%	-79.2	64%	-63.9	71%	-88.4	60%
3C4	-228	-21.6	91%	-71.2	69%	-54.8	76%	-86.3	62%
3C5	-219	268	222%	254	216%	234	207%	128	158%
4C1	-101	89.3	188%	26.2	126%	60.4	160%	32.8	132%
4C2	-106	-21.3	80%	-35.0	67%	-28.0	74%	-38.4	64%
4C3	-104	-19.6	81%	-33.2	68%	-25.0	76%	-37.0	64%
4C4	-106	-13.7	87%	-33.0	69%	-24.1	77%	-38.7	63%
4C5	-102	50.4	149%	59.5	158%	47.3	146%	20.5	120%

9.1.3 SELECTED LINEAR ELASTIC JOINT RESPONSE

In addition to stress ratios, the forces and displacements at a selected joint were isolated and compared for the two models. The selected joint (joint 4J2 in **Figure 8-1**) exhibited a marked fracture of the column flange at the beam-to-column connection (see **Figures 4-5, 4-6,** and **4-11**) and was selected as a representative joint for more detailed study.

Table 9-3 compares the maximum elastic forces in the members framing into joint 4J2 for each of the six analyses. For dynamic analyses, the maximum forces are those that occur over the entire record and do not necessarily occur concurrently in all of the members or for a given member end. The forces in **Table 9-3** refer to the notation given in **Figure 9-3**; all forces are absolute values.

TABLE 9-3: MAXIMUM LINEAR ELASTIC FORCES AT JOINT 4J2

Member/Force	*2D Static*	*2D Dynamic (Site)*	*2D Dynamic (Newhall)*	*3D Static*	*3D Dynamic (Site)*	*3D Dynamic (Newhall)*
4C2 M_z (in-k)	3591	25820	20790	3995	24390	18920
4C2 F_x (k)	64.00	81.33	71.44	63.56	72.60	63.47
4C2 F_y (k)	44.23	319.1	256.6	49.10	300.7	233.2
3C2 M_z (in-k)	4944	41180	32550	5316	37760	28800
3C2 F_x (k)	144.3	161.8	167.4	145.2	157.9	152.9
3C2 F_y (k)	62.19	517.2	409.0	67.08	474.6	362.0
4G1 M_z (in-k)	5010	31700	23990	5400	27920	23250
4G1 F_x (k)	76.70	74.80	55.55	68-72	216.6	183.8
4G1 F_y (k)	55.87	305.9	223.1	59.90	256.6	229.5
4G2 M_z (in-k)	2973	31740	25950	3311	30130	21210
4G2 F_x (k)	58.80	245.8	182.9	49.45	156.7	129.6
4G2 F_y (k)	18.71	291.7	237.6	21.39	276.8	180.8

Table 9-3 reinforces the stress ratio results, showing a large increase in force for the dynamic analyses. The shears and moments in the girders and columns are most significantly affected by the dynamic loading. In some instances (e.g., the moment in Girder 4G2), the dynamic analysis produce elastic forces that are an order of magnitude larger than the equivalent static analysis. Note that in the companion experimental study at the University of Minnesota, girder moments of approximately 10,000 to 15,000 in-k (i.e., on the order of the moment capacity of the W27x94) were applied to the specimens to induce failure. Section 9.2.5 investigates the nonlinear response on this beam-to-column connection region, and plots the resulting moment-rotation response of one of the girders framing into it.

FIGURE 9-3: GIRDER-TO-COLUMN CONNECTION NOTATION

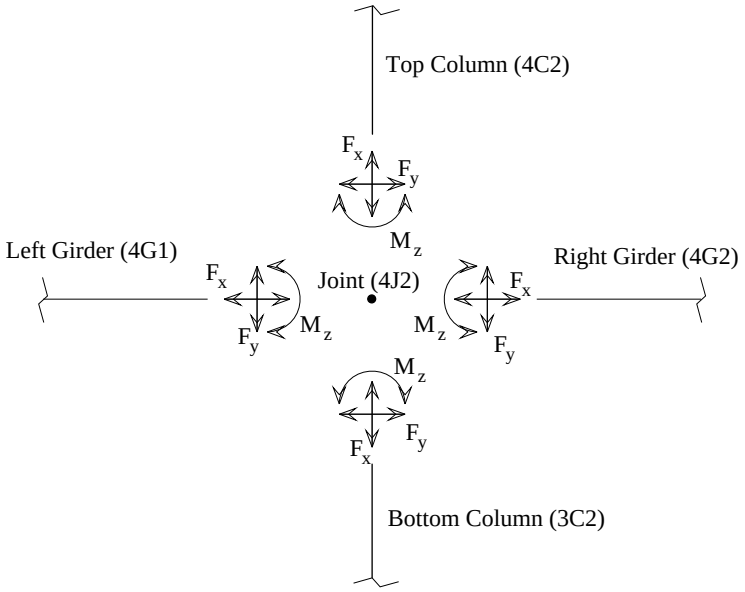

9.1.4 CORRELATION OF LINEAR ELASTIC RESULTS WITH FAILURE LOCATIONS

A primary objective of performing the elastic analyses is to attempt to correlate the results with locations of failure in the structure. The force levels due to elastic analysis, as reported above, indicate that in all likelihood this structure was subjected to significant material inelasticity. Nevertheless, the forensic study of the Borax building, as well as of a number of other affected steel structures in the area (Yousef et al. 1995), has indicated that it is possible that minimal inelastic deformation occurred up to the point of failure for many of the connections which failed in the Northridge earthquake. This is possibly due to strain rate effects or triaxial stresses in the weld region. If this is indeed the case, an elastic analysis may provide an indication of potential problem connections.

Table 4-3 shows the percentage of bottom flange connections on each floor that were damaged. This table illustrates the primary trend exhibited by the failures in the structure, i.e., the number of connection failures increased toward the base of the structure. The failures within a given floor did not exhibit any definitive patterns, i.e., the exterior connections did not exhibit more failures, or more severe failures, than the interior connections, or vice versa.

Examining the stress ratios shown in **Figures 9-1** and **9-2**, along with the damage summaries of **Figure 4-11**, indicates that the column stress ratios increase more substantially in the lower floors, which correlates well with the observed damage patterns. The girder stress ratios from the 2D dynamic analysis show a similar pattern, although they also show a bias towards having larger stresses at the exterior of column lines of the frame. However, the 3D analyses show little pattern in their girder stress ratios. As will be shown in Section 9.2.3, the 2D and 3D analyses

generally yield similar behavior for the full duration of their time histories, although they deviate from each other sufficiently to result in the variations between, for example, their maximum elastic stress ratios. Thus, while the correlation between the 2D transient dynamic elastic results and the observed damage is reasonably good, the correlation of the 3D analyses with the damage is weaker. Nevertheless, the results from these analyses suggest that either large column stresses, or the combination of large column stresses and large girder stresses in a linear elastic time-history analysis, may be indicative of potential connection failures.

9.2 SECOND-ORDER INELASTIC ANALYSES

The inelastic analyses of the two models examine the fully nonlinear dynamic response of the structure, including modeling of nonlinear behavior due both to material and geometric (e.g., P-Δ and P-δ) effects. In addition to the dynamic analyses of the 2D and 3D frames, a static inelastic "pushover" analysis of the 2D and 3D frames is performed. The primary objectives of the second order inelastic analyses are to: 1) assess the ductility of the structure under seismic loading by examining member rotational and story displacement ductilities; 2) examine global displacements and forces and compare the response of the full 3D structure with the 2D moment frame; 3) examine the response of an isolated connection as was done in Section 9.1 by looking at forces and moment-rotation curves; and 4) correlate the inelastic results with observed failure locations in the structure by investigating rotational and story ductilities, and distributions of forces.

The static pushover analyses of the two frames follow the load patterns described in Section 8.3. Gravity loads of $1.2D + 0.5L$ are applied, followed by lateral loads, which are distributed throughout the frame as per UBC-88 (see Section 8.3). The lateral loads are increased from zero until the structure either reaches a target roof displacement value or collapses due to a combination of geometric and material nonlinearity. The target displacement, which is used as an estimate of the maximum displacement the frame will experience under a given earthquake, may be determined in a number of ways (Lawson et al., 1994). In this study, the target displacements for the pushover analyses were established as the maximum roof displacements of the 2D and 3D frames for the fully nonlinear dynamic analyses using the Site accelerogram. However, in both analyses, the structures collapse before the target displacements are reached. The 2D model becomes unstable at a load factor of 2.0 times the base equivalent static loads, with a roof displacement of 9.2 in., or 1.40% drift (versus a maximum displacement of 15.4 in., or 2.34% drift, for the 2D Site analyses). The 3D model becomes unstable at a load factor of 2.36 times the equivalent static loads, with a roof displacement of 12.9 in., or 1.96% drift, (versus a maximum displacement of 14.6 in., or 2.22% drift, for the 3D Site analysis). Global displacements will be discussed further in Section 9.2.3. The earlier collapse of the frames in the pushover analyses stems in part from the larger gravity loads on the columns (gravity loads of $1.2D + 0.5L$ are applied in the pushover analyses versus $1.0D + 0.5L$ in the dynamic analyses). In addition, the static load application causes a more monotonic progression of yielding in the frame than the dynamic analyses, which in turn causes all of the frame members which are

highly stressed to exhibit a simultaneous loss in their stiffnesses with increased loading. Also, as with any transient dynamic analysis, the inertial effects of the mass may effectively stabilize the structure (from a numerical standpoint), thus delaying numerical instability that may otherwise be detected in a static analysis (through detection of an indefinite coefficient matrix).

9.2.1 ROTATIONAL DUCTILITY RATIOS

Rotational ductility is used as a means of detecting connections in the structure that undergo significant deformation. In this report rotational ductility is measured about the major axis of the member and is defined as the ratio of the total member end major axis rotation to the member end major axis rotation at initial yield. Computation of the rotational ductility ratio for a member end therefore requires the determination of the rotation at the yield point of the member.

Recall from Section 7 that the plasticity formulation is based upon a two-surface bounding surface model, in which the size of the inner loading surface and the outer bounding surface are specified as a percentage of the size of the characteristic cross-section strength surface of the member. To detect the yield rotation for a member, the same concept of a surface in three-dimensional force space is employed here. Also recall from Section 7 that the loading surface indicates the onset of inelastic behavior (e.g., accounting for residual stresses), but that much of the member stiffness is retained after contact with the loading surface. Therefore, since little plastic deformation occurs directly after contact with the loading surface, for the purpose of assessing rotational ductility, it is preferable to construct a yield detection surface at the point where rapid softening tends to initiate in a wide-flange member, rather than the point of initial inelastic behavior (i.e., contact with the loading surface). A convenient value to use for the size of this yield detection surface (denoted φ) is the ratio of the major axis yield moment, M_{xy}, to the major axis ultimate moment, M_{xo}. This ratio may be simplified to the ratio of the elastic modulus, S_x, to the plastic modulus of the section, Z_x, which is the inverse of the familiar shape factor of a section. The yield detection coefficient φ may thus be summarized as follows:

$$\varphi = \frac{M_{xy}}{M_{xo}} = \frac{f_y \cdot S_x}{f_y \cdot Z_x} = \frac{S_x}{Z_x} \tag{9-2}$$

where f_y is the yield stress of the material. The value of φ is typically between 0.8 to 0.9 for most wide-flange sections. This value is a more accurate indication of the onset of significant plastic rotation than 0.5, the size of the loading surface, and is used in this work for ductility computations.

Rotational ductility ratios were computed for all girders and columns in each of the inelastic analyses and are shown in **Figures 9-4** and **9-5**. The girder rotations used for these ductilities are evaluated at the intersection of the girder end and its rigid link. The column rotations are those at the main joints of the frame (shown in **Figure 8-1**). These figures enumerate the maximum values of these ratios in a similar manner to the elastic stress ratios shown in **Figures 9-1** and **9-**

2. **Figure 9-4** shows the rotational ductility ratios for girders in the 2D frame. The top values for each member apply to the static pushover analysis. The second and third values apply to the Site dynamic analysis and the Newhall dynamic analysis, respectively. The dynamic analysis values are member maximums over the entire record and do not necessarily occur concurrently in all of the members. Similar maximum ductility ratios are given in **Figure 9-5** for the west north-south moment frame of the 3D model. Blank entries in these figures indicate that the member end remained elastic throughout the analysis.

FIGURE 9-4: MAXIMUM INELASTIC ROTATIONAL DUCTILITY RATIOS -- N-S MOMENT FRAME OF 2D STRUCTURE

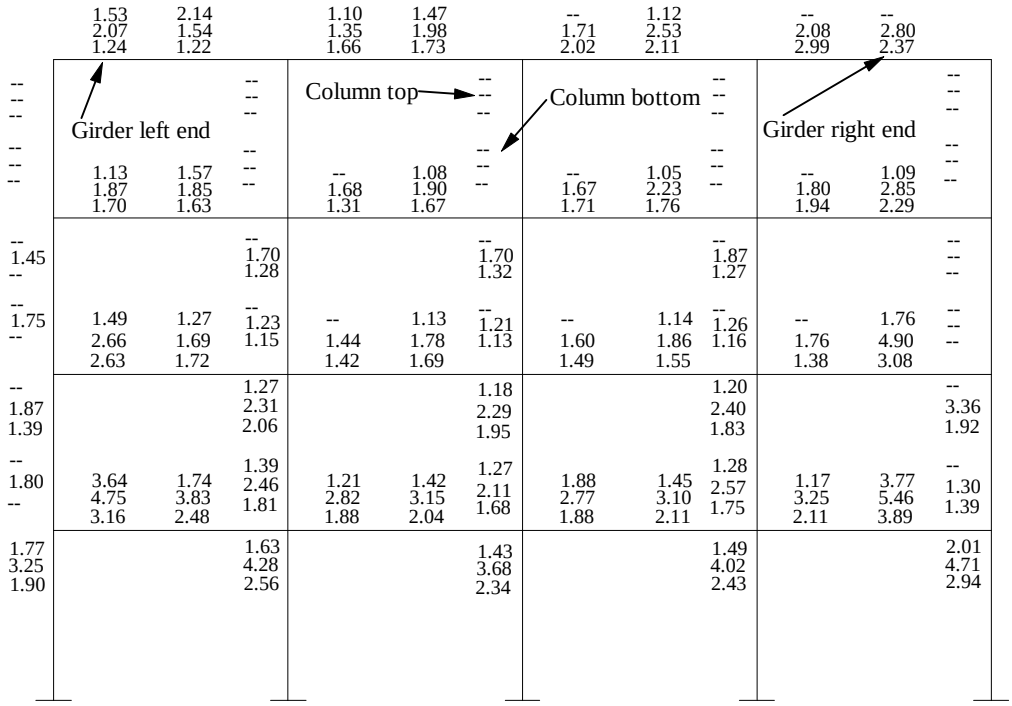

1) Static Pushover

2) Dynamic -- Site Record

3) Dynamic -- Newhall Record

Figures 9-4 and **9-5** illustrate the extensive yielding of the girders and columns in all of the analyses, with ductility values above 3.0 not uncommon. Every girder in the frame behaves inelastically at some point during both dynamic analyses for both frames. For the equivalent static analyses, all but a few of the girder ends away from the applied load (i.e., on the south end of the frame) in the 2D frame become inelastic. The column ductility ratios, in turn, decrease with elevation for all analyses, with several of the upper story columns remaining elastic during the analyses. The ductility ratios shown in the dynamic analyses occurred over extensive time periods and did not merely occur at isolated points in time.

FIGURE 9-5: MAXIMUM INELASTIC ROTATIONAL DUCTILITY RATIOS -- N-S MOMENT FRAME OF 3D STRUCTURE

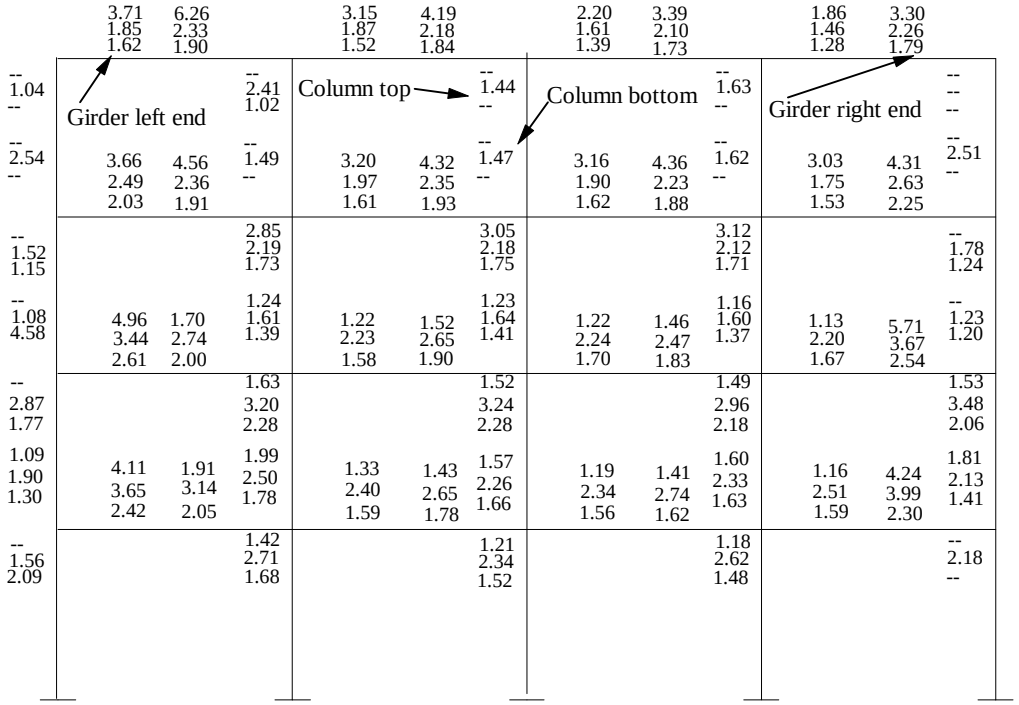

1) Static Pushover
2) Dynamic -- Site Record
3) Dynamic -- Newhall Record

However, the girder ductilities due to the pushover analyses, and in particular the 3D static analysis, increase substantially with elevation, and they are larger for the exterior connections than the interior. Because the equivalent lateral load is largest at the roof (see **Table 8-1**), the amount of inelastic deformation predicted in the upper floor girders is significant in the static analyses. This does not correlate with the observed damage. The girder ductility ratios from the 2D dynamic analyses and the 3D dynamic analysis using the Newhall accelerogram show somewhat better correlation with the observed damage, although the pattern of the maximum ductility ratios for each of these analyses is somewhat sporadic. However, the 3D inelastic transient dynamic analysis using the Site accelerogram shows strong correlation with the observed damage. The maximum girder rotational ductilities occur at the second and third floors, with the ductility demands in the upper floor girders being only somewhat smaller. In addition, these results show a lower range of maximum ductility values across any given floor than the static analyses or the 2D transient dynamic analyses -- this also correlates well with the observed damage of **Figure 4-11**. Finally, while the column ductility ratios decrease with elevation for all analyses, only the 3D inelastic dynamic analyses show a clear trend of having larger ductility demands at the top of the column below each joint (i.e., in the critical region near

the bottom flanges of the girders, where the fracturing occurred), as compared to the bottom of the column above each joint.

The strong correlation of these rotational ductility demands points to the potential influence of inelastic redistribution on the behavior of this structure. While the amount of inelastic deformation which occurred in the Borax building may not have been substantial prior to the connections fracturing (see Section 4), it is clear that some redistribution of force, either due to inelasticity or to fracture, must have occurred in this structure, given the magnitude of forces seen in the dynamic analyses. The measure of ductility demand exhibited in these analyses provides a strong indication of which portions of the structure were required to withstand significant straining. The elastic analyses did not identify as clearly the dominance of ductility demand in the interior column lines of the lower stories of the west N-S moment frame. Perhaps more importantly, the static pushover analyses did not indicate the probable redistribution of force with the height of the structure, especially since the equivalent lateral load procedure traditionally emphasizes potential high lateral shears in the upper stories of the structure (Lawson et al., 1994, have made similar observations). Only after inelastic redistribution had taken place during the 3D inelastic transient dynamic analyses did the ductility demands of the girder and column ends show the clearest correlation with the observed damage. In the Borax building, it is the first two floors that took the brunt of the damage, with the upper floors sustaining significant but somewhat less damage, and with all earthquake-related fractures occurring in the region of the bottom flanges of the girders. The 3D transient dynamic inelastic analysis using the Site record identifies these trends unequivocally.

9.2.2 INTERSTORY DISPLACEMENT DUCTILITY

In addition to ductility on the member level, ductility may also be examined on the global structural level by computing interstory and total structural displacements. **Table 9-4** lists the maximum interstory displacement ductility ratio in each story for the six inelastic analyses. The interstory displacement ductility ratio is measured as the total story displacement (i.e., the north-south displacement measured at the exterior joint of the moment frame for each analysis--joint 2J1 for story one, joint 3J1 for story two, etc.) divided by the floor displacement at the initiation of significant yielding (as defined in Section 9.2.1) in any of the members of the floor. For example, the first story displacement ductility for the 2D frame subjected to Site accelerations is given as 4.45 in **Table 9-4**. This indicates that joint 2J1 displaces 4.45 times the displacement that caused the first instance of significant yielding in either the first story columns or the second floor girders.

If the girder rotational ductilities of Section 9.2.1 are reexamined, the patterns of larger rotational ductilities correspond with the results in **Table 9-4** as expected, since large story displacements will produce correspondingly large girder rotational ductility demands. All three 2D analyses result in large inelastic displacements in the first floor relative to higher floors. While this shows some correlation with the observed damage, a more uniform decrease in the interstory drift

ductilities would be expected. The 3D static analysis, in turn, produces the largest interstory ductility in the top floor, which correlates with the large girder rotational ductilities exhibited in the previous section, again due primarily to the distribution of the equivalent lateral loads.

TABLE 9-4: MAXIMUM INTERSTORY DISPLACEMENT DUCTILITY RATIOS

Story	*2D Static Pushover*	*2D Dynamic (Site)*	*2D Dynamic (Newhall)*	*3D Static Pushover*	*3D Dynamic (Site)*	*3D Dynamic (Newhall)*
1	3.15	4.45	2.52	2.36	2.81	1.80
2	1.69	2.47	2.11	3.19	2.84	1.98
3	1.15	1.59	1.87	2.87	2.01	1.81
4	1.66	1.45	1.80	3.68	1.88	1.68

The 2D Newhall analysis and both 3D transient dynamic analyses exhibit distributions of interstory ductility that correspond most closely with the observed damage in the Borax building. The 3D transient dynamic analyses in particular show the most uniform distribution of interstory drift ductilities throughout the height of the structure, and thus they best reflect the observed damage.

9.2.3 GLOBAL AND STORY DISPLACEMENTS

Figure 9-6 illustrates the roof displacements versus time for each of the four inelastic dynamic analyses. The roof displacement is measured as the displacement of node RJ1 (see **Figure 8-1**) in the north-south direction (in **Figure 9-6**, north is shown as positive displacement and south is shown as negative displacement).

The 2D and 3D analyses produce similar displacement versus time curves for both the Site record and the Newhall record, both in magnitude and pattern (similar close correlation is seen in the time histories of the forces of the two models). This indicates that the 2D analysis reasonably simulates the total behavior of the 3D model, even though the distribution of displacements and ductilities throughout the height of the structure is ultimately somewhat different in the two models. The Site analyses show large excursions in the north direction, but both models damp out with residual displacements in the south direction. This points out that it is not necessarily the magnitude of displacements, but the pattern of yielding that determines residual displacements. Also, Lawson et al. (1994) demonstrated that very strong ground motions may result in no residual displacement in a steel frame structure, while considerably weaker accelerations result in large residual displacements. **Table 9-5** summarizes the residual displacements for the four inelastic dynamic analyses.

FIGURE 9-6: INELASTIC ROOF DISPLACEMENT VS. TIME

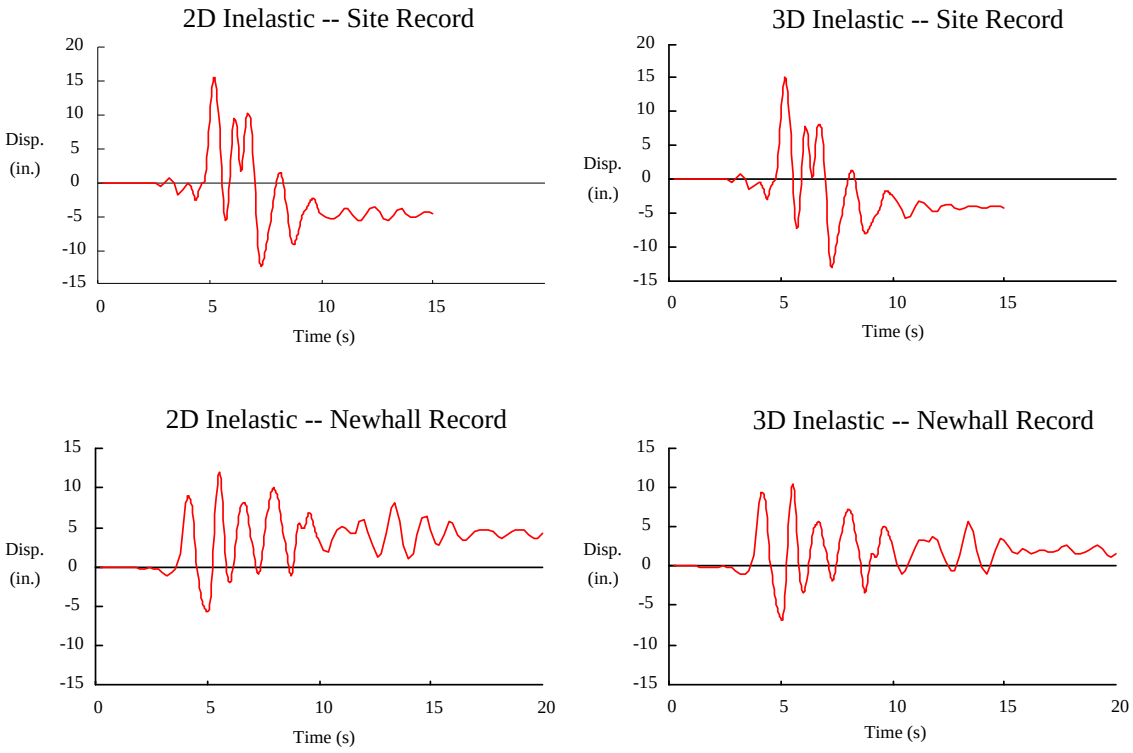

TABLE 9-5: RESIDUAL ROOF DISPLACEMENTS

Direction	*2D Dynamic (Site)*	*2D Dynamic (Newhall)*	*3D Dynamic (Site)*	*3D Dynamic (Newhall)*
North-South	5.9 in. South	3.7 in. North	4.0 in. South	1.4 in. North
East-West	--	--	0.73 in. West	0.78 in. East

The actual out-of-plumbness of the structure after the Northridge earthquake was shown in **Table 4-4**. The roof displaced 2.04 inches to the south and an average of 1.38 inches to the west. If the residual displacement values from the inelastic analyses in **Table 9-5** are compared to these measured values, the 3D dynamic analysis using the Site record shows the best correlation. The Newhall record produces residual roof displacements in directions opposite the measured values. These results, although seemingly accurate for the Site record, should be viewed with discretion, since structural components such as stairwells and annexes, which are not modeled explicitly here, may have a significant effect on residual displacements.

Perhaps more important are the maximum displacements in a dynamic analysis. For the static analyses, **Figure 9-7** plots the deflection of each story in the frame with respect to the applied load factor. For the dynamic analyses, **Table 9-6** summarizes the maximum roof displacements.

TABLE 9-6: MAXIMUM ROOF DISPLACEMENTS

Direction	*2D Dynamic (Site)*	*2D Dynamic (Newhall)*	*3D Dynamic (Site)*	*3D Dynamic (Newhall)*
North	15.4	11.9	14.6	10.5
South	13.0	5.95	12.8	6.57
East	--	--	6.55	7.38
West	--	--	5.29	4.67

Table 9-7 isolates each floor for the six inelastic analyses and shows the maximum absolute value of interstory displacements for the west north-south moment frame in each case. **Figure 9-8** illustrates the same results as cumulative maximum displacement envelopes (i.e., displacement at each floor level is the maximum displacement relative to the base of the structure). For the dynamic analyses, these plots are envelopes in the sense that the maximum displacement values at each floor in an analysis do not necessarily occur concurrently in the time history of the earthquake.

As discussed in the previous sections, **Figure 9-8** shows that the 2D analyses tend to exhibit greater displacements in the lower story levels, whereas the 3D analyses exhibit a more uniform displacement along the entire height of the structure, which correlates better with the observed damage.

TABLE 9-7: MAXIMUM INTERSTORY DISPLACEMENTS

Story	*2D Static Pushover*	*2D Dynamic (Site)*	*2D Dynamic (Newhall)*	*3D Static Pushover*	*3D Dynamic (Site)*	*3D Dynamic (Newhall)*
1	4.05	7.28	3.85	2.55	4.26	2.52
2	2.24	3.95	3.28	3.94	4.69	3.11
3	1.49	2.38	2.62	3.62	3.62	2.95
4	1.36	1.57	1.74	2.83	2.31	2.16

FIGURE 9-7: STATIC LOAD VS. INELASTIC STORY DISPLACEMENTS

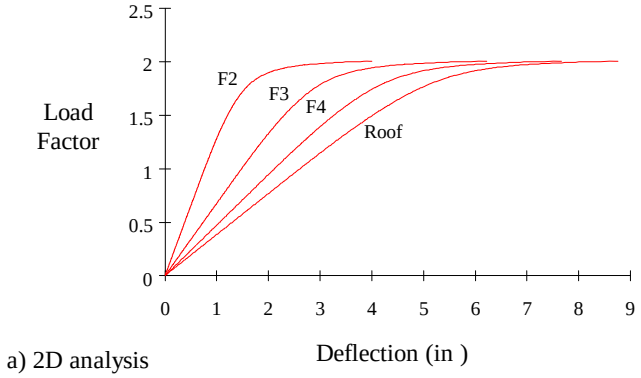

a) 2D analysis

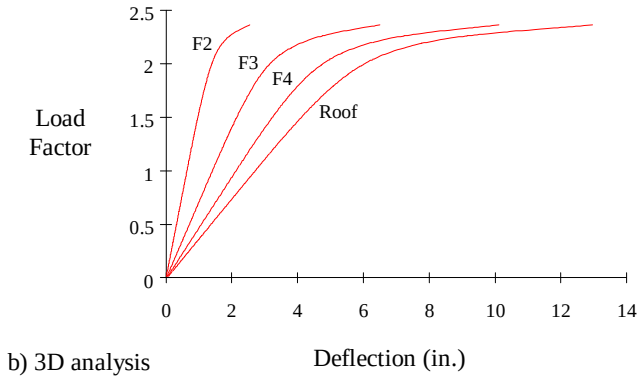

b) 3D analysis

FIGURE 9-8: MAXIMUM DISPLACEMENT ENVELOPES

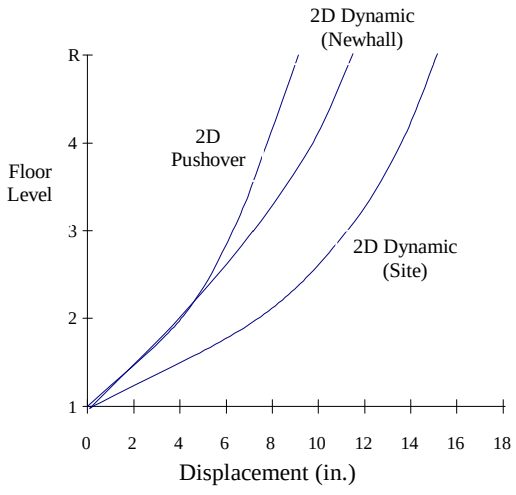

a) 2D Analysis

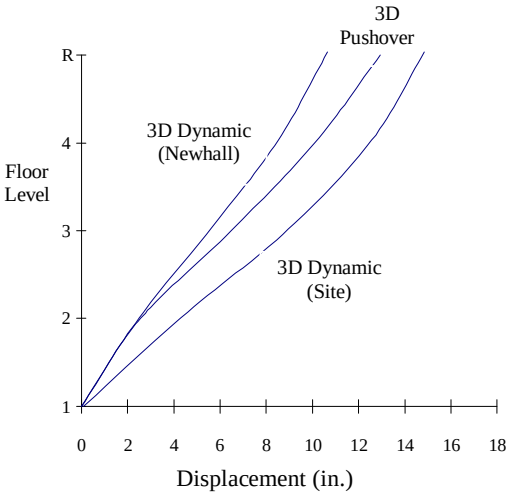

b) 3D Analysis

9.2.4 TENSILE AXIAL COLUMN FORCE

Table 9-8 lists the maximum axial forces in the columns of the Borax building in a manner identical to that used to generate **Table 9-2**. Comparing the results to those of **Table 9-2**, one may see that the results of inelastic redistribution are significant: the maximum tensile loads in the structure are substantially reduced. Nevertheless, these results clearly indicate the potential that relatively low compressive forces, or possible tensile forces, existed throughout the moment frame columns for significant portions of the earthquake.

TABLE 9-8: SECOND-ORDER INELASTIC TENSILE AXIAL COLUMN FORCES
(NEGATIVE FORCE VALUE INDICATES COMPRESSION)

Column Notation (see Figure 8-1)	*Gravity Load, GL (k) 1.0D + 0.5L*	*2D Dynamic (Site)*		*2D Dynamic (Newhall)*		*3D Dynamic (Site)*		*3D Dynamic (Newhall)*	
		Max. force (k)	*% of GL*	*Max. force (k)*	*% of GL*	*Max. force (k)*	*% of GL*	*Max. force (k)*	*% of GL*
1C1	-446	210	147%	175	139%	291	165%	249	156%
1C2	-474	-87.2	82%	-110	77%	-46.5	90%	-126	73%
1C3	-460	-88.3	81%	-94.8	79%	-97.0	79%	-98.3	79%
1C4	-472	-63.2	87%	-47.8	90%	-77.7	84%	-57.5	88%
1C5	-452	188	142%	122	127%	306	168%	154	134%
2C1	-331	151	146%	113	134%	222	167%	199	160%
2C2	-351	-72.4	79%	-80.2	77%	7.30	102%	-56.5	84%
2C3	-341	-93.0	73%	-82.3	76%	-20.9	94%	-45.2	87%
2C4	-350	-58.7	83%	-49.7	86%	-11.0	97%	-24.4	93%
2C5	-335	147	144%	88.3	126%	249	174%	78.1	123%
3C1	-217	69.4	132%	36.4	117%	109	150%	105	148%
3C2	-228	-54.6	76%	-54.0	76%	6.29	103%	-35.2	85%
3C3	-223	-49.3	78%	-60.3	73%	-7.51	97%	-30.0	87%
3C4	-228	-36.6	84%	-42.5	81%	-15.8	93%	-21.1	91%
3C5	-219	70.8	132%	29.9	114%	140	164%	16.6	108%
4C1	-101	14.0	114%	-0.21	100%	35.4	135%	33.9	134%
4C2	-106	-20.7	80%	-22.2	79%	-2.60	98%	-12.3	88%
4C3	-104	-17.7	83%	-26.0	75%	-8.02	92%	-12.4	88%
4C4	-106	-18.3	83%	-17.5	83%	-5.99	94%	-11.2	89%
4C5	-102	15.8	115%	-1.87	98%	42.8	142%	-6.00	94%

9.2.5 SELECTED INELASTIC JOINT RESPONSE

Table 9-9 compares the maximum inelastic forces in the members framing into joint 4J2 for each of the six inelastic analyses. For the dynamic analyses, the maximum forces are those that occur over the entire record and do not necessarily occur concurrently in all of the members or for a given member end. The forces in **Table 9-9** refer to the notation given in **Figure 9-3**; all forces are absolute values.

TABLE 9-9: MAXIMUM INELASTIC FORCES AT JOINT 4J2

Member / Force	*2D Static Pushover*	*2D Dynamic (Site)*	*2D Dynamic (Newhall)*	*3D Static Pushover*	*3D Dynamic (Site)*	*3D Dynamic (Newhall)*
4C2 M_z (in-k)	7009	9715	9217	9956	11067	10791
4C2 F_x (k)	63.97	77.48	65.03	63.39	86.58	90.92
4C2 F_y (k)	82.55	121.3	114.8	119.1	136.4	132.7
3C2 M_z (in-k)	10182	12494	12317	12720	12983	12377
3C2 F_x (k)	145.1	161.5	143.7	145.7	181.0	191.5
3C2 F_y (k)	127.4	157.2	154.6	159.8	158.6	154.6
4G1 M_z (in-k)	8522	9839	9689	9723	9945	9870
4G1 F_x (k)	153.9	32.81	31.42	140.5	115.2	109.9
4G1 F_y (k)	91.26	102.5	102.4	103.6	103.1	100.8
4G2 M_z (in-k)	7618	9906	9546	9902	9956	9710
4G2 F_x (k)	109.8	94.29	74.38	91.57	105.2	108.8
4G2 F_y (k)	57.90	102.3	89.51	73.82	93.13	91.40

If **Table 9-9** is compared to the elastic forces in **Table 9-3**, it is readily evident that, in the dynamic analyses, member yielding serves to relieve member forces and distribute the forces to other locations in the structure. For a given type of loading, the inelastic forces are on the order of one third of the elastic values shown in **Table 9-3**. However, it is also illustrative to compare the inelastic 3D dynamic analysis for the Site record with the linear elastic static analysis of the 2D frame. The 3D dynamic analysis may be considered the most representative model of the actual building, whereas the 2D static analysis typifies the type of analysis used in the design of the moment frames. If the results from the two analyses are compared for this selected joint, the forces in the 3D joint are on average two to three times the magnitude of the elastic forces. The moments show the greatest disparity. Column moments increase from an average of 4300 in-k in the 2D analysis to an average of 12,000 in-k in the 3D analysis; girder moments increase from 4000 in-k to 8050 in-k. Column shears also increase significantly in the more detailed analysis, rising for the bottom column from 62 k in the 2D analysis, to 160 k in the 3D analysis. Note that the moments resulting from the dynamic analyses are relatively close in magnitude to the moments applied in the corresponding experimental studies of these steel beam-to-column connections.

Figure 9-9 illustrates the moment-rotation curves for this joint, generated from the 3D transient dynamic analyses of the structure. These plots are representative of the moment-rotation exhibited at many of the frame's joints in these analyses. As mentioned in Section 4, many researchers have suggested that two strong pulses may have induced the connection failures. These moment-rotation curves indicate, for both ground motions, two substantial changes in member rotation (e.g., for the Site record, a maximum rotation of 4 mrad is obtained after a first significant plastic excursion, followed by a more substantial excursion on the order of 6 mrad). Note that the rotations exhibited in this member (and in most of the members of this structure) are well below the level of 20 mrad or more that should be required to cause significant damage to this connection detail.

FIGURE 9-9: MOMENT-ROTATION CURVES FOR JOINT 4J2

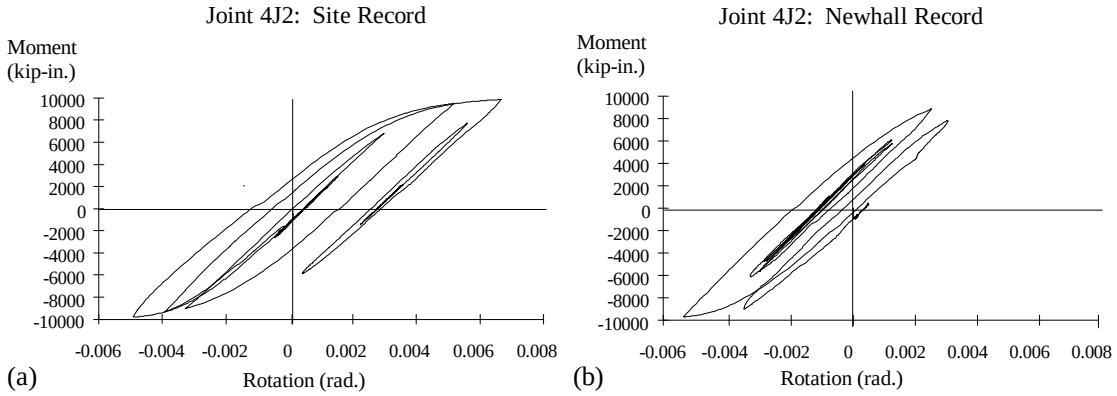

10. CONCLUSIONS

Seventy-five percent of the moment connections in the Borax building suffered brittle fractures during the Northridge Earthquake and, in most cases, there was no evidence of accompanying ductile deformation. The bulk of the damage apparently occurred as a result of a strong long period pulse attributable to rupture directivity. Although the site ground motions produced demands on the connections significantly higher than those anticipated by the building code, brittle fracturing was unexpected.

It is now widely accepted that the primary cause of the moment connection fractures discovered following the Northridge Earthquake was a fundamental flaw in the standard pre-qualified welded-flange bolted-web connection prescribed in the building code. At the Borax building, welding flaws, local stress concentrations due to continuity plate detailing and construction, and possibly embrittlement of the HAZ were also contributing factors, but their relative importance is unknown. Limited redundancy of the structure probably also served to increase the extent of the damage. As mentioned in Section 3, many of the exterior columns in the north-south frames and all of the interior building columns were not designed to participate in the lateral load

resisting system. Consequently, when fractures occurred, the increased demand on the remaining intact connections was substantially greater than it would have been had the system been highly redundant.

All of the Borax building's second floor framing moment connections suffered fractures at the location of the bottom girder flange, and forty percent of the moment frame shear connection plates were damaged. Additionally, the fractures in some of the shear connection plates noticeably grew during aftershocks. The building had obviously lost most of its lateral capacity and was unsafe to occupy. More importantly, had the duration of strong ground motion been longer, it is quite possible that at least partial collapse could have occurred.

The moment connection damage was more prevalent in the north-south frames, with eighty-six percent of the their connections damaged versus sixty percent of the east-west frame connections. This is consistent with the stronger estimated site ground motions in that direction. One striking difference, however, was observed between the failure types in the two directions. Ninety-five percent of all column flange fractures (Damage Types C4 and C4*) occurred in the north-south direction. This suggests that more energy input may be required to produce column fractures than the other failure types.

The set of twelve two-dimensional and three-dimensional, linear and nonlinear, static and transient dynamic frame analyses of the Borax building support the findings of the forensic investigation, and they provide insights into the pros and cons of using these various types of analysis for seismic behavioral evaluation and design. The results reported for these analyses focus on the north-south moment frame on the west side of the structure, as that frame's damage was extensive. Several conclusions may be drawn from these results.

First, as may be expected, the girder and column stress ratios resulting from the elastic static analysis using code-specified equivalent lateral loads were substantially smaller than those resulting from elastic transient dynamic analyses, using both a site-specific three-dimensional accelerogram and the accelerograms recorded at the nearby Newhall Fire Station. In addition, the patterns of maximum member stress ratios exhibited in the elastic static analyses do not correlate with the observed damage. Results from the inelastic static "pushover" analyses also do not correlate well with the observed damage, as they show strong dependence on the distribution of the equivalent lateral loads, which thus creates higher forces in the upper floors of the structure, where damage in the actual structure was somewhat lighter.

Results from the transient dynamic analyses show better correlation. However, while the stress ratios from the 2D elastic transient dynamic analyses do decrease with increasing elevation in the structure, they under-emphasize the significant straining exhibited in the interior column lines of the lower floors of the west north-south moment frame, where the severest damage occurred. The 3D elastic dynamic analyses and 2D inelastic dynamic analyses similarly show inadequate correlation with the damage.

Alternately, the 3D inelastic transient dynamic analyses, particularly the analysis based upon the use of the site-specific ground acceleration, show strong correlation with the observed damage, based on both member and story-level displacement ductility measures, as well as an assessment of residual deformation in the structure: the girder and column ductility ratios decrease moderately with increasing building height, with the top floors still clearly showing straining levels sufficient to cause damage; the ratios are relatively constant across any given floor; and the column inelastic deformation demands are more severe at the top of each column, in the critical region of the bottom girder flanges, as compared to at the bottom of the column.

Evidence of large inelastic excursions was not found in the forensic study of the Borax building. In addition, neither the girder and column rotational ductilities, nor the maximum rotations at the girder ends, were excessively large in the 3D inelastic dynamic analyses. However, the ductility demands and elastic force levels obtained from these analyses are sufficient to indicate substantial redistribution of forces may have occurred either due to fracture or inelasticity, or a combination of both, during the course of the seismic excitation, and that this redistribution had a substantial effect on the final pattern of failures observed in the structure. The analytical studies also strongly indicate the possibility that the columns in this structure were subjected to axial tension, or small levels of axial compression, during significant portions of the seismic excitation. All of these findings point to the fact that this structure, while designed properly to meet code, was subjected to significant force and deformation levels that its basic structural configuration could not withstand.

The strengthened connections in the Borax building are capable of resisting significantly greater moment demands. However, since the precise configuration used (column size, beam size, strengthening rib sizes) has not been tested, it is not possible to determine whether the connections are capable of withstanding the rotational ductility demands likely to be imposed by future strong ground motion.

ACKNOWLEDGMENTS

Funding for this research was provided by the Federal Emergency Management Agency through the SAC Joint Venture. SAC is a partnership of the Structural Engineers Association of California, the Applied Technology Council, and California Universities for Research in Earthquake Engineering. Portions of this research were also funded by the National Science Foundation (Grant No. CMS-9416363) under Drs. Shih-Chi Liu and M. P. Singh, the American Institute of Steel Construction, the University of Minnesota, and the Georgia Institute of Technology. The authors gratefully acknowledge this support. Statements made in this publication do not necessarily reflect the views of the SAC Joint Venture or the Federal Emergency Management Agency, who are not responsible for any losses sustained as a result of the use of information or guidance contained in this publication.

The authors would like to thank Dr. Paul G. Somerville, Woodward Clyde Consultants, for providing site-specific accelerograms for this project, Mr. David L. Norris, Western Inspection and Testing Services, whose forensic photographs were invaluable in describing the fractured connections, and Mr. Patrick F. Carlson, University of Minnesota, for his assistance in preparing some of the figures and tables in this document.

REFERENCES

Darragh, R., Cao, T., Cramer, C, Huang, M., and Shakal, A. (1994). "Processed CSMIP Strong-Motion Records From the Northridge, California Earthquake of January 17 1994: Release No. 1," Report No. OSMS 94-06B, California Strong Motion Instrumentation Program, California Department of Conservation, Division of Mines and Geology, Office of Strong Motion Studies, 48 pp.

Engelhardt, M. D. and Husain, A. S. (1993). "Cyclic-Loading Performance of Welded Flange - Bolted Web Connections", *Journal of Structural Engineering*, ASCE, Vol. 119, No. 12, pp. 3537-3550.

Gourley, B. C. and Hajjar, J. F. (1994). "Cyclic Nonlinear Analysis of Three-Dimensional Concrete-Filled Steel Tube Beam-Columns and Composite Frames," Structural Engineering Report No. ST-94-3, Department of Civil Engineering, University of Minnesota, Minneapolis, Minnesota, 216 pp.

Hilmy, S. I. (1985). "A Strain-Hardening Concentrated Plasticity Model for Nonlinear Dynamic Analysis of Steel Buildings," *NUMETA 85, Numerical Methods in Engineering: Theory and Applications*, Vol. 1, pp. 305-314.

Lawson, R. S., Vance, V., and Krawinkler, H. (1994). "Nonlinear Static Push-Over Analysis--Why, When, and How?," Proceedings of the Fifth U.S. National Conference on Earthquake Engineering, July, 10-14 1994, Chicago, Illinois, Earthquake Engineering Research Institute, Oakland, California, Vol. 1, pp. 283-292.

Orbison, J. G., McGuire, W., and Abel, J. F. (1982). "Yield Surface Applications in Nonlinear Steel Frame Analysis," *Computer Methods in Applied Mechanics and Engineering*, Vol. 33, pp. 557-573.

Orbison, J. G. (1982). "Nonlinear Static Analysis of Three-Dimensional Steel Frames." Ph.D. dissertation, Department of Civil Engineering, Cornell University, Ithaca, NY, 243 pp.

Popov, E. P. and Stephen, R. M. (1972). "Cyclic Loading of Full-Size Steel Connections," *Steel Research for Construction*, Bulletin No. 21, American Iron and Steel Institute, New York.

Popov, E. P., Amin, N. R., Louie, J. C., and Stephen, R. M. (1985). "Cyclic Behavior of Large Beam-Column Assemblies," Earthquake Spectra, Vol. 1, No. 2, pp. 203-238.

SAC Joint Venture (1995). *Interim Guidelines: Evaluation, Repair, Modification, and Design of Welded Steel Moment Frame Structures,* Federal Emergency Management Agency & State of California Governor's Office of Emergency Services.

Somerville, P. G., Graves, R. W., and Saikia, C. K. (1995). "Characterization of Ground Motions at the Sites of Subject Buildings," Report on Task 4 of the SAC Joint Venture Project.

White, D. W., and Hajjar, J. F. (1991). "Application of Second-Order Elastic Analysis in LRFD: Research to Practice." *Engineering Journal,* AISC, Vol. 28, No. 4, pp. 133-148.

Woodward Clyde Consultants (1994). "Ground Motion Evaluation for the Borax Site, Santa Clarita, California," Internal Report, Woodward Clyde Consultants, Santa Ana, California.

Yousef, N., Bonowitz, D., and Gross, J. (1995). "A Survey of Steel Moment-Resisting Frame Buildings Affected by the 1994 Northridge Earthquake," Report No. NISTIR 5625, Building and Fire Research Laboratory, National Institute of Standards and Technology, Gaithersburg, Maryland.

Zhao, Y. (1993). "Modeling of Inelastic Cyclic Behavior of Members, Connections, and Joint Panels of Steel Frames," Ph.D. dissertation, Department of Civil Engineering, Cornell University, Ithaca, New York, 197 pp.